INFLUENCE OF MECHANICAL CONDITIONS DRIVING CLINICAL PERFORMANCE OF MEDICAL DEVICE CONSTRUCTS AND SYSTEMS: A DUAL-STUDY APPROACH IN HUMAN AND VETERINARY FIELDS FOR OPTIMIZATION OF THE CLINICAL OUTCOME

A Dissertation

by

STEVE ZAMBRANO

Submitted to the Office of Graduate and Professional Studies of
Texas A&M University
in partial fulfillment of the requirements for the degree of

DOCTOR OF PHILOSOPHY

Chair of Committee,	Michael R. Moreno
Committee Members,	W. Brian Saunders
	John C. Criscione
	Balakrishna Haridas
Head of Department,	Michael McShane

December 2017

Major Subject: Biomedical Engineering

ABSTRACT

The work performed focused on the investigation of human and veterinary orthopedic devices. The work was accomplished in two parts and focused on different device aspects, with emphasis on biomechanical implications.

Part I covers the design, development, and implementation of a novel joint motion replicator and was divided into two sections: (a) Joint Motion Replicator design and development, and (b) Joint Motion Replicator implementation in a toggle rod construct ex vivo study application. The replicator provides a dual-axis, closed-loop, stepper-controlled mechanical testing environment capable of reproducing physiologically relevant loading conditions and dynamic processes. Additionally, the ex vivo study compared biomechanical performance of three toggle rod fixation systems using cyclical testing protocols simulating flexion/extension and abduction/adduction.

Part II of this work covers human implantable orthopedic devices, specifically devices used to treat fifth metatarsal base fractures located at the metaphyseal-diaphyseal watershed junction (Jones fractures). This project compares the biomechanical performance of a well-known intramedullary screw construct with a plantar-lateral plating construct applied to replicated Jones fractures in paired cadaver foot specimens.

DEDICATION

To tears, sleep-depravity, and Oakley, my companions who held my hand through the longest and most tumultuous parts of completing a doctoral degree. You will always be remembered.

ACKNOWLEDGEMENTS

I would like to thank my committee chair, Dr. Michael R. Moreno, and my committee members, Dr. W. Brian Saunders, Dr. John C. Criscione, and Dr. Balakrishna Haridas, for their guidance and support throughout this research.

Additionally, thanks to my mother for always believing in me and nurturing me. *Sin su ayuda, nada de esto hubiera sido posible!* To my father, I indirectly credit you for being the inception of my love and passion for engineering, for without your excessive over-protectiveness I may never have had the yearning to break, build, and explore; everything build up in me so feverishly. To my sisters Rosa, Melba, Maricela, and Lisa, you all in your own ways have impacted my educational career. Thanks also go to Richard P., my friends, colleagues, and the department faculty/staff for making my time at Texas A&M University a great experience. The students that I have mentored, whether they know it or not, have been a source of personal fulfillment that I hope will flourish into a lifelong network of professionals and friends. I also want to extend my gratitude to the Sloan Foundation Fellowship, which provided me with a place to be among understanding peers.

Finally, I would like to reflect on those long nights that blended into early mornings or those never-ending obstacles of life that I overcame. It was my drive…my perseverance…my work ethic which kept me going. It is my hope to look back on this document, years from now, and fully appreciate the person that I have become while reminiscing about how this life's chapter has influenced who I am.

CONTRIBUTORS AND FUNDING SOURCES

Contributors

This work was supervised by a dissertation committee consisting of Professor Michael R. Moreno of the Department of Mechanical Engineering, Professor W. Brian Saunders of the Department of Small Animal Clinical Sciences, Professor John C. Criscione of the Department of Biomedical Engineering, and Professor Balakrishna Haridas of the Department of Biomedical Engineering.

Regarding the *Development and Verification of a Joint Motion Replicator to Evaluate Joint Kinematics in a Bio-Replicative Environment*, work for this dissertation was completed by the student in collaboration with:

- Dr. W. Brian Saunders of the Department of Small Animal Clinical Sciences,
- Christopher Leidlein, and Joshua Corso of the Department of Biomedical Engineering
- Nathan Dunkelberger of the Department of Mechanical Engineering.

Regarding the *Comparison of Three Modified Toggle Suture Constructs for Craniodorsal Hip Luxation in Dogs: An Ex Vivo Cyclical Biomechanical Study*, work for this dissertation was completed by the student in collaboration with:

- Dr. Jodie Lamb, and Dr. W. Brian Saunders of the Department of Small Animal Clinical Sciences

- Dr. Marcelo W. Teixeira, a visiting scholar of the Rural Federal University of Pernambuco.

Regarding the *Development of an Environmental Chamber for Biosafety Level 2 Human Cadaver Testing*, work for this dissertation was completed by the student in collaboration with:

- Aaron C. Stone of the Department of Mechanical Engineering

Regarding *A Biomechanical Comparison of Fifth Metatarsal Jones Fracture Fixation Methods-What is the Ideal Construct?*, work for this dissertation was completed by the student in collaboration with:

- Dr. Neil Duplantier, and Dr. Ronald Mitchell of the Houston Methodist Orthopedics and Sports Medicine Research Group
- Aaron C. Stone of the Department of Mechanical Engineering.

Funding Sources

Graduate study was supported by a fellowship from the Alfred P. Sloan Foundation. Regarding the *Development and Verification of a Joint Motion Replicator to Evaluate Joint Kinematics in a Bio-Replicative Environment* and *Comparison of Three Modified Toggle Suture Constructs for Craniodorsal Hip Luxation in Dogs: An Ex Vivo Cyclical Biomechanical Study*, this work was made possible by a Dr. Michael R. Moreno Startup Fund [Department of Mechanical Engineering, Texas A&M University], Ginn Fund

[Department of Small Animal Clinical Sciences, Texas A&M University] and the Bone and Joint Fund [Texas A&M Foundation].

Regarding *Development of an Environmental Chamber for Biosafety Level 2 Human Cadaver Testing,* this work was made possible by this work was made possible by a Dr. Michael R. Moreno Startup Fund [Department of Mechanical Engineering, Texas A&M University].

Regarding *A Biomechanical Comparison of Fifth Metatarsal Jones Fracture Fixation Methods-What is the Ideal Construct?,* this work was made possible, in part, by Arthrex, Inc. through a supported research agreement for allocation of orthopedic fracture fixation devices. This work was also sponsored via a research agreement with Houston Methodist Orthopedics and Sports Medicine Research Group.

NOMENCLATURE

A/A	Abduction/Adduction
AOR	Axis of Rotation
ASD	Average Standard Deviation
BW	Body Weight
CTF	Cycles to Failure
DOF	Degree of Freedom
E/E	Endorotation/Exorotation
EB	Ethibond Excel with Hand-Turned Knowles Toggle System
F/E	Flexion/Extension
FHO	Femoral Head Ostectomy
GW	Gap Width
JMR	Joint Motion Replicator
MN	Monofilament Nylon with Securos Toggle System
PFL	Peak Failure Load

PLA	Poly [Lactic Acid]
PMMA	Poly [Methyl Methacrylate]
RMS	Root Mean Square
ROM	Range of Motion
SD	Standard Deviation
THR	Total Hip Replacement
TR	Tightrope Joint Stabilization System
TSC	Toggle Suture Construct

TABLE OF CONTENTS

Page

LIST OF FIGURES

Page

LIST OF TABLES

Page

1. INTRODUCTION

This dissertation work is designed to address biomechanical concerns in human and veterinary medicine, specifically with respect to implantable orthopedic devices. Recently, there has been great interest in the One Health initiative. According to the One Health vision statement: "One Health (formerly called One Medicine) is dedicated to improving the lives of all species—human and animal—through the integration of human medicine, veterinary medicine and environmental science." One Health is essentially a multidisciplinary approach to improving health across species – human and animal medicine – and the relationship between species and the ecosystem. One of the goals of the One Health paradigm is the removal of "silos", wherein those from different disciplines traditionally operate in isolation from those that might share common or complimentary concerns, skills, resources, etc. Removing these silos and integrating work across disciplines has the potential to produce unique and enabling capabilities, skills, and expertise [1]. The work was focused on the development and investigation of human and veterinary implantable orthopedic devices. Though it is not uncommon for animal models of human pathology to be employed in developing a medical technology, it is important to note that the animal work described herein is actually designed for veterinary application. The work was accomplished in two parts and will focus on different aspects of device development with specific emphasis on the biomechanical implications.

Part I of this work covers the development, and application of a novel joint motion replicator; it has been divided into two sections. The system was designed specifically for veterinary applications – a purpose that distinguishes it from commercially available biomechanical testing systems. The joint motion replicator (JMR) provides a dual-axis, closed-loop, stepper-controlled mechanical testing environment capable of reproducing physiologically relevant loading conditions and dynamic processes. With modification, the system could be deployed to test orthopedic devices, total joint replacements, ex vivo joint specimens, and synthetic phantoms. In this work, a canine hip testing protocol was developed for a comparative study of existing commercially available implantable devices designed to treat hip luxation in canines.

Part II of this research focuses on human implantable orthopedics, specifically devices and methods used to treat fifth metatarsal base fractures located at the metaphyseal-diaphyseal watershed junction, also known as a Jones Fracture. This research consists of two sections, (1) design and development of a mechanical testing system with an environmental chamber, and (2) a biomechanical performance comparison of an intramedullary screw and plantar-lateral plate construct applied to replicated Jones Fractures in paired cadaver foot specimens. The purpose of the environmental chamber was to allow for a variety of load-testing applications and to implement safety features to reduce the potential risk of infectious or bodily injury associated with loading the samples to failure.

2. VETERINARY ORTHOPEDIC BIOMECHANICS

The project covering veterinary orthopedic biomechanics is focused on the development of a custom load frame capable of producing physiologically relevant reconstructions of the mechanical environment of the canine hip through normal daily activity, i.e. flexion-extension, adduction-abduction. The system allowed fatigue testing of TSC technologies in canine cadaver specimens of the hip joint, including the pelvis and femur. The system allows for imaging confirmation alignment of the motion axes. Furthermore, the system also allows the bone-device constructs to be tested in saline at physiologic temperature.

2.1 Development and Verification of a Joint Motion Replicator to Evaluate Joint Kinematics in a Bio-Replicative Environment

Ex vivo simulation of active joint motion is useful to evaluate rehabilitation protocols and surgical procedures in the laboratory prior to their application in patients [2, 3]. This section presents a development and performance evaluation of a new joint motion replicator (JMR).

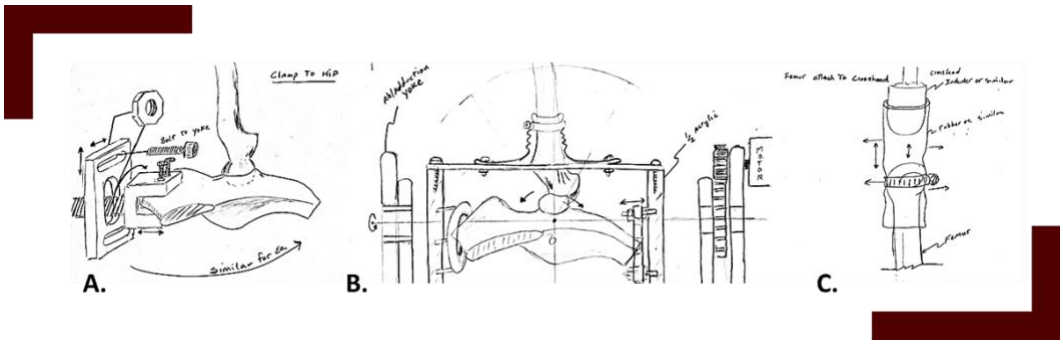

Figure 1: (A.) pelvic clamp mechanism with rotation feature concept, (B.) environmental chamber in replicator frame, and (C.) attachment concept of replicator loading arm to distal aspect of femur

The need for dynamic motion replication is apparent in biomedical research as evidenced by the numerous existing devices, machines, and load frames, which aim to replicate specific physiologic systems. However, the cost associated with this equipment generally increases with the specificity of the replicator. The objectives for the development of the JMR were to: (1) provide a cost effective alternative to traditional dynamic motion replication devices, (2) provide a modular framework that could be used for several applications (3) replicate relevant flexion/extension (F/E) motion profiles on the primary axis and abduction/adduction (A/A) motion profiles on the secondary axis, (4) incorporate the ability to maintain physiologically relevant environmental conditions, (5) enable in situ radiography, and (6) provide accurate and repeatable simulations. The JMR allows the user to replicate a variety of dynamic motion applications with only minor modifications. The capabilities of the JMR have been outlined through validation testing for several different parameters and testing conditions. JMR validation consisted of three

tests. First, accuracy and repeatability were quantified for straight line and sinusoidal movements. Second, the JMR's ability to replicate a physiologically relevant motion profile was tested by simulating the motion of a canine coxofemoral joint, showing how a physiologic motion profile compares to the straight line and sinusoidal movement profiles. Third, two curve-fit algorithms were tested to discover the preferable option in different testing scenarios. A case study is also analyzed, comparing several TSC models that are used to repair luxation in a canine coxofemoral joint. The maximum errors for the replicator during validation remained below 0.7° for straight line motion testing, 4.0° for sinusoidal motion testing, and 1.2° for canine hip motion testing. The Root Mean Squared (RMS) errors remained below 0.6° for straight line motion testing, 2.6° for sinusoidal motion testing, and 0.6° for canine hip motion testing. The ASDs remained below 0.4° for straight line motion testing, 2.0° for sinusoidal motion testing, and 0.8° for canine hip motion testing. The curve-fit algorithm testing resulted in the Cubic B Spline being used for future testing. These results outline the JMR's ability to replicate physiologic motion profiles under relevant environmental conditions provided by the environmental chamber. The modularity of the replicator allows different physiologic systems to be tested, providing an economic alternative to system specific replicators.

2.1.1 Introduction

An understanding of the relationship between dynamic physiologic motion and the response of the body is crucial to further the knowledge of biological responses. Evaluation of orthopedic therapies, rehabilitation procedures, and injury prevention are

largely dependent on access to relevant data gained from models, simulations, and replications of physiologic scenarios.

Computational modeling is a frequently used method to model the reaction of tissues to physiologic loads. While computational models are useful in many simplified cases, it is extremely difficult to create accurate models of biological materials [4-8].

There are many commercially available motion replication devices and load frames for biomedical research, but many of these devices have drawbacks which limit their use to specific applications. Such devices [9, 10] are often highly specialized toward one specific class of applications, limiting their utility. These devices and systems often require a complete redesign to replicate conditions that are only slightly different from the primary application. Additionally, because the intent of these systems is to precisely replicate a specific condition, the cost associated with this equipment generally increases as the specificity of the motion and dynamics increases [11]. Joint replicators should aim to reproduce physiologically relevant forces and motion to mimic the way that joints behave in vivo [11-13]. The JMR aims to accomplish this by meeting the following design requirements:

1. Provide a cost effective alternative to traditional dynamic motion devices and load frames
2. Provide a modular framework that can be used for several applications

3. Replicate relevant Flexion/Extension motion profiles on the primary axis and Abduction/Adduction motion profiles on the secondary axis
4. Incorporate physiologically relevant environmental conditions
5. Enable in situ radiography
6. Provide accurate and repeatable dynamic motion scenarios

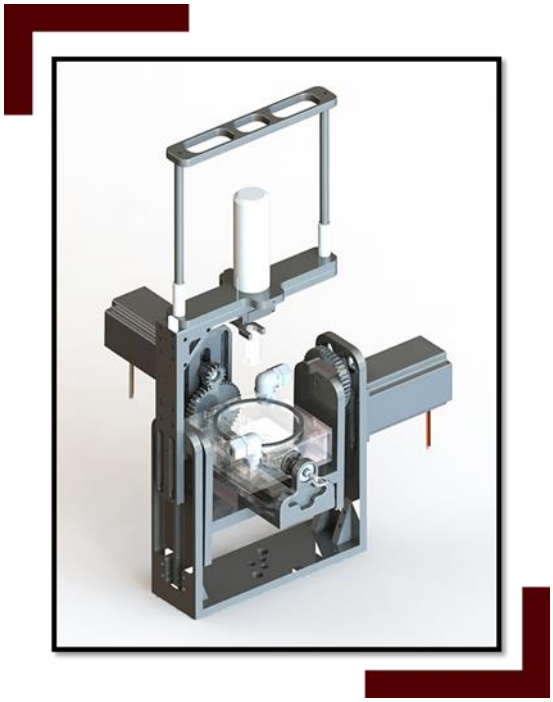

Figure 2: Component design and assembly modeling was developed using Dassault Systèmes SOLIDWORKS

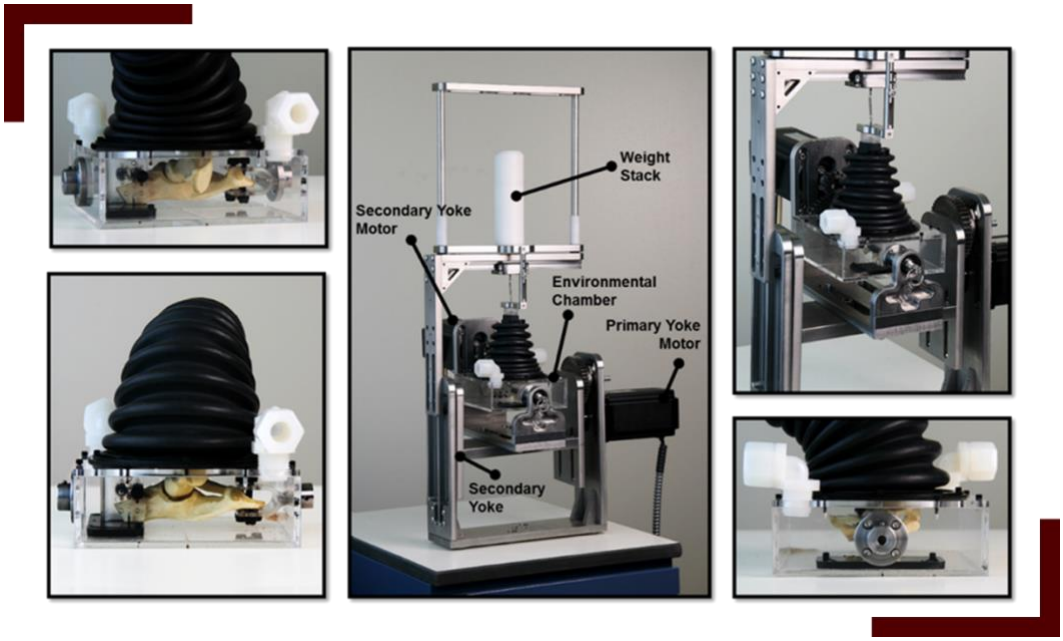

Figure 3: The JMR with important features labeled - when used in testing, the bottom of the frame is mounted to remain stationary

The JMR is cost effective compared to other system-specific motion replicators and it is applicable for a wider variety of testing situations. As a part of a laboratory, this dynamic motion replicator can be used for multiple research projects with replacement of system specific hardware modules. Because the replicator has biaxial rotation capabilities, it is suited to emulate physiologically relevant motions and test multiple scenarios (e.g. rotary cuff surgery, cruciate ligament research, coxofemoral joint motion recreation). The replicator has been utilized for testing Toggle Suture Constructs (TSCs) in the canine coxofemoral joint, but it has the potential for use in many other applications.

In this chapter, (a) device design and components are outlined, (b) the replicator is validated by testing the performance under various motion profiles (c) canine coxofemoral joint simulation is reviewed as a case study, and (d) further implications of the replicator will be discussed.

2.1.2 Materials & Methods

The replicator is a dual-axis, closed-loop, system composed of two sub-systems. The first subsystem is a custom assembly consisting of two 303 stainless steel yokes mounted to a frame of the same material. This yoke-system mounts in series to a dead-load rack system. Motion of the primary and secondary yokes is accomplished via two stepper motors coupled to independent drivers and power supplies. Due to the complex motion profiles required and need for future expansion, an NI cRIO-9076 integrated controller and chassis was chosen. This, paired with the motion control software LabVIEW SP1 and NI SoftMotion, allows for highly configurable motion profiles such as coordinated or concurrent movements that can be reconfigured and expanded to include additional sensors as future experiment applications require.

Primary & Secondary Yokes

The primary and secondary yokes are shown in Fig. 1. Each yoke uses a high-torque stepper motor with encoder and motor driver (National Instruments; Austin, TX; SMD 7620) as the source of motion with its own DC power supply (National Instruments; Austin, TX; NI PS 16). Each motor driver is set to a micro stepping configuration of

20,000 steps per revolution. There is a locating laser mounted along the Axis of Rotation (AOR) of each of the yokes which allows the joint to be placed precisely at the AOR of the motor, thereby reducing misalignment errors. Additional specifications for each yoke are included in Table 1.

Table 1: Detailed yoke specification

Yoke	Motor	Motor Torque (oz-in)	Gear Ratio	Range of Motion (min, max) (degrees)
Primary	NI ST34-9E	1694	1:2.8	-55, 35
Secondary	NI ST34-3E	555	1:3	-55, 55

This replicator is capable of active flexion/extension (F/E) and abduction/adduction (A/A) motions. Motion control was achieved via a combination of fixtures and actuators attached to relevant sample locations. Replicated active flexion will be compared to passive flexion in terms of repeatability, motion pathways and joint laxity.

In order to more closely replicate the physiologic environment of the canine hip, an integrated environmental chamber for housing specimens during testing was developed. This chamber was required to have certain functionalities to accommodate the needs of both engineers and clinicians. Features include:

- One-movement chamber release

- Radio-transparent chamber body and fixtures
- Modular design to allow for swappable specimen clamping mechanisms
- Sound structure at cyclical loading (≤ 75 lbs.) and static loading (≤ 125 lbs.)
- Laser alignment with the joint replicator frame
- Saline immersion and cycling throughout the chamber

Figure 2 below shows an early prototype of the chamber.

The last component of the replicator is a real-time control loop that controls the coxofemoral joint angle for both F/E and A/A motions. Motion of the primary and secondary yokes is accomplished via the two high-torque stepper motors coupled to independent drivers (National Instruments, SMD-7620) and power supplies (National Instruments, NI PS-16). Due to the complex nature of the motion profiles required and need for future expansion, an NI cRIO-9076 integrated controller and chassis was chosen. This paired with the motion control software (National Instruments, LabVIEW 2013 SP1 & NI SoftMotion) allows for highly configurable motion profiles including coordinated and concurrent movements. Figure 3 shows the motion control hardware.

Fixture Attachment

Because the JMR was designed for a variety of applications, it was important to include a user-friendly method for attaching different testing fixtures. As part of the secondary yoke, an easily configurable system is implemented to allow designed fixtures to be interchanged. On the motor-side, a square pin is located at the center of the output gear.

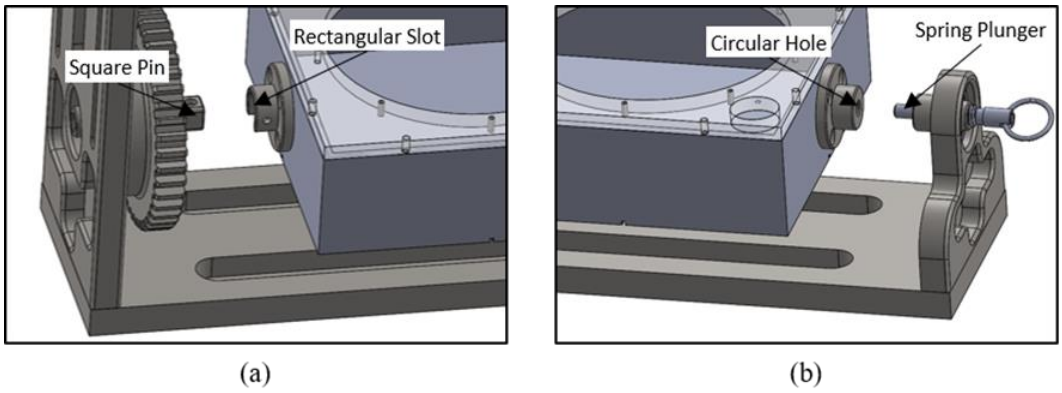

Figure 4: Fixture attachment to the secondary yoke for (a) motor side and (b) yoke

As shown in Figure 4, to attach the fixture to the yoke, a rectangular slot slides onto the square pin. This ensures that the fixture stays in line with the motor. On the opposite side, there is a ball bearing with a spring plunger attached. On the fixture, a circular hole is used as the connection to the spring plunger, as depicted in Figure 4, with a set screw normal to the spring plunger acting as a locking mechanism. The bearing allows the fixture to rotate freely with the gear throughout simulation.

Environmental System

In the initial case study, the JMR included an environmental chamber. The chamber was filled with a saline solution (0.9% Sodium Chloride) to replicate the fluids that are present in orthopedic joints. A heated recirculator pump (Polyscience; Niles, IL; 210) regulated the fluid at canine body temperature (38-39.2 °C). The JMR's ability to incorporate an environmental chamber provides an advantage over existing simulation devices. This is

especially relevant in kinematic studies since the lack of properly replicated lubrication can often lead to inaccurate conclusions [14].

In the JMR configuration, the chamber included a soft-shell bellows which allowed clinicians to gain real-time tactile feedback from the bone as it underwent motion simulation. Additionally, the radio-transparent enclosure allowed clinicians to assess cadaveric materials with the fixture intact. Incorporating radio-opaque cross-hair markers within the chamber allowed the cadaver to be accurately positioned via radiologic assessment of the cadaver-fixture construct. In this case study, clamps were designed to hold the ischial and iliac pelvic regions of the cadaver. Other environmentally controlled housings can be implemented to fit the JMR as mentioned in the Fixture Attachment Section.

Modular Frame

With modularity in mind, the frame was designed with the ability to easily add or modify existing components. This was crucial to the goal of making a truly configurable test bed. The bolt-pattern on the baseplate of the frame allows for a universal mounting adapter, enabling the device to be mounted to load frames. The frame holds the dead-load rack system which includes the measurement tools, the dead-load weights, and the distal cadaver mount. This system allows for interchangeable modules and components that can be used for different testing purposes, such as testing of human joints. Additional uses are discussed in the Future Work section of this article.

Dead-Load Rack System

To replicate contact forces to the joint, a dead-load rack system (Fig. 1) mounted on a Delrin® low-friction bushing, has been implemented. The rack configuration allows for the addition of weight plates while maintaining unconstrained vertical displacement. The motion of the system would be substantially hindered without this feature. Preserving vertical mobility is especially important when considering the potential variability between test specimens, since the replicator can test different sized cadavers without requirement to alter the configuration. When F/E and A/A motions occurred, variations in skeletal geometries caused translational motion to occur. If a constrained rack system was used, translational motion would not be allowed and force premature dislocation.

Equipment Configuration

For our case study testing, the prepared hemipelvis was first inserted into the custom-designed environmental chamber (Figure 3). Pelvic vises were used to secure each hemipelvis, and the chamber lid was secured to the chamber box with a gasket. The femur's free end and the bellows' open end were secured into a femoral pot, creating a closed environment for the cadaver specimen. The cadaver-filled environmental chamber was mounted, as mentioned in the Fixture Attachment section. The lasers, which were mounted along each AOR, were used to align the joint precisely with the JMR's axes. Similar methods could be used to fixate other physiologic systems with an environmental chamber.

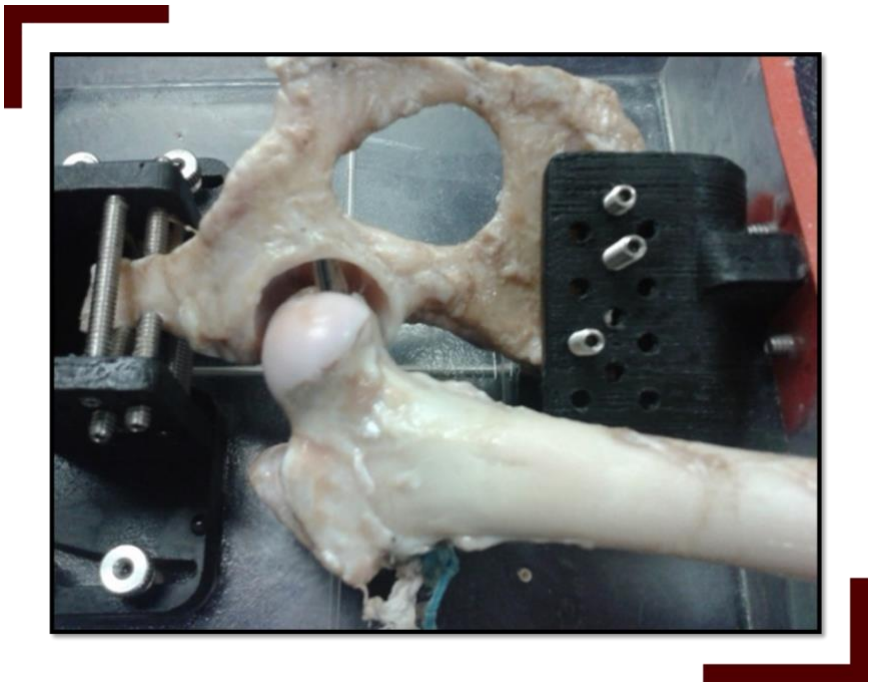

Figure 5: Cadaver fixturing - the hemipelvis was held in place by the pelvic vises and the femur was fixed to the hemipelvis through TSC attachment by a clinician following standard surgical procedures

Hardware

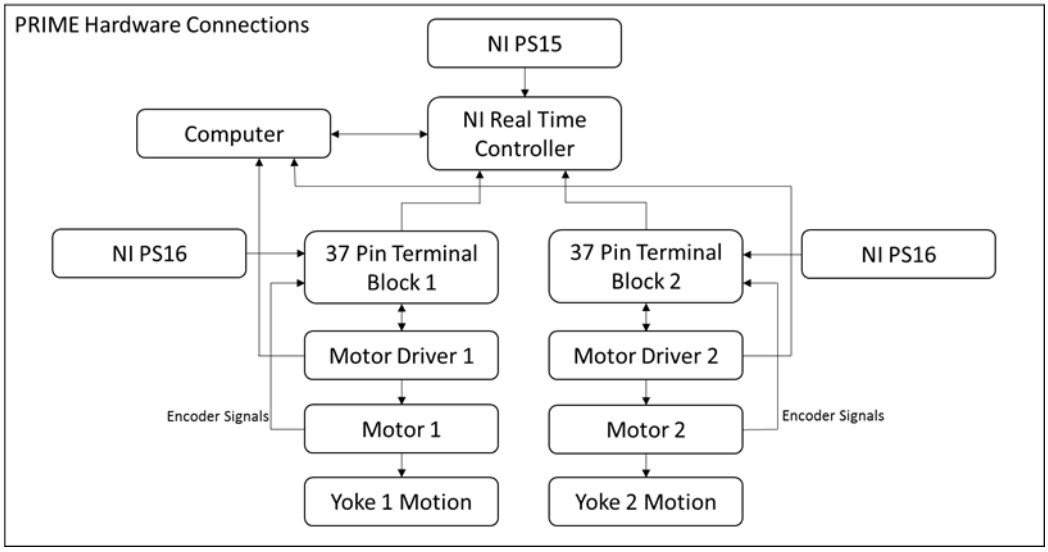

Figure 6: Schematic of hardware components interface

Software

The encoders in each motor provide real-time feedback to the computer to regulate the desired output. Motors are controlled by LabVIEW's built in Softmotion control algorithm. This uses an FPGA to optimize system performance. A schematic of the electronics used is shown in Figure 6.

The JMR program was developed using National Instruments LabVIEW 2013 SP1 software, and NI softmotion. These programs allow for custom motion control: an important prerequisite for outputting complex motion profiles to the replicator. In particular, the JMR's ability to replicate coordinated and concurrent movements is crucial to meeting the design requirement of simulating relevant motion profiles.

For the testing of the coxofemoral joint, the salient data were the mode of failure and the number of cycles to failure or the end of the trial. Because these results may not be applicable to each kind of testing situation, the output is configurable to the desired quantities. The quantities that are currently available include angular position, angular velocity, and angular acceleration at each time step, and the number of iterations. Other desired quantities can be easily added to interface with LabVIEW.

Validation Methods & Setup

Several characterization tests were performed to define the general system capabilities and evaluate the JMR's ability to perform mechanical testing on a physiologic system. The replicator was tested using an injection molded model of the canine coxofemoral joint to accurately replicate motion constraints.

Accuracy & Repeatability Testing Methods

The first test that was performed quantified the accuracy and repeatability of the replicator in following a predefined motion profile. Testing was performed on each yoke independently, and with both yokes operating concurrently. Each of the test scenarios were performed in multiplicity (n = 10) to understand how the replicator behaves over several tests. For each set of tests, the first predefined motion profile was a sinusoidal waveform with an amplitude of 50° and a frequency of 0.5 Hz. A sinusoidal wave was chosen because it is a simplified motion profile that has been adopted by several replicator validation studies as a standard of motion characterization. Therefore, results can be

compared across multiple studies [2, 3, 15]. The second motion profile chosen to test was a straight line move of 50° at approximately 13°/s, with the start and end points determined by the physiologic orientation of the canine coxofemoral joint model. The sinusoidal and straight-line motion profiles characterize the replicator motion response under minimal and fluctuating motion conditions. Each of these testing profiles were tested unloaded and loaded with 25 lbf (111.2 N).

To quantify the accuracy of the system, the RMS error was calculated for each testing scenario. The repeatability of the replicator was measured by assessing the average standard deviation (ASD) for each test scenario. Accuracy and repeatability results are displayed graphically as a bulk resultant of all ten tests for each testing scenario (Fig. 6-8). The RMS error, maximum error, and ASD for each testing scenario are displayed numerically in.

Canine Coxofemoral Joint Testing Methods

To test the replicator's ability to reproduce physiologically relevant motions, the replicator was tasked with reproducing F/E and A/A ROMs of a canine coxofemoral joint. These motion profiles were adopted from literature on three dimensional kinematic analyses for canine gait [16]. As with the accuracy and repeatability evaluation, testing was performed for each yoke individually, then with both of the yoke motion profiles concurrently. Each scenario was tested unloaded and loaded with 25 lbf (111.2 N). The primary yoke was used for the F/E motion profile while the secondary yoke was used for the A/A motion

profile because the primary yoke has a larger ROM. The performance of the replicator was quantified through the accuracy and repeatability measures outlined in the previous section. Multiple trials were run (n = 10) to understand how the replicator behaves over several tests. The data gathered for the physiologically relevant motions was compared to the data gathered from the previous tests, including the RMS errors, maximum errors, and ASDs of the replicator. This data is displayed graphically (Fig. 8-10) and numerically in with the accuracy and repeatability testing results.

2.1.3 Results

Accuracy & Repeatability

The maximum errors for the replicator remained below 0.7° for straight line motion testing, 4.0° for sinusoidal motion testing, and 1.2° for canine hip motion testing. The RMS errors remained below 0.6° for straight line motion testing, 2.6° for sinusoidal motion testing, and 0.6° for canine hip motion testing. The ASDs remained below 0.4° for straight line motion testing, 2.0° for sinusoidal motion testing, and 0.8° for canine hip motion testing. A portion of the results are displayed graphically, (Fig. 6-8) showing the input motion profile and the mean output motion profile ±1 SD. The maximum error, RMS error, and ASD for each testing condition are also shown in table format (Table 3). Graphs of the other 20 loading scenarios can be found in the supplementary data.

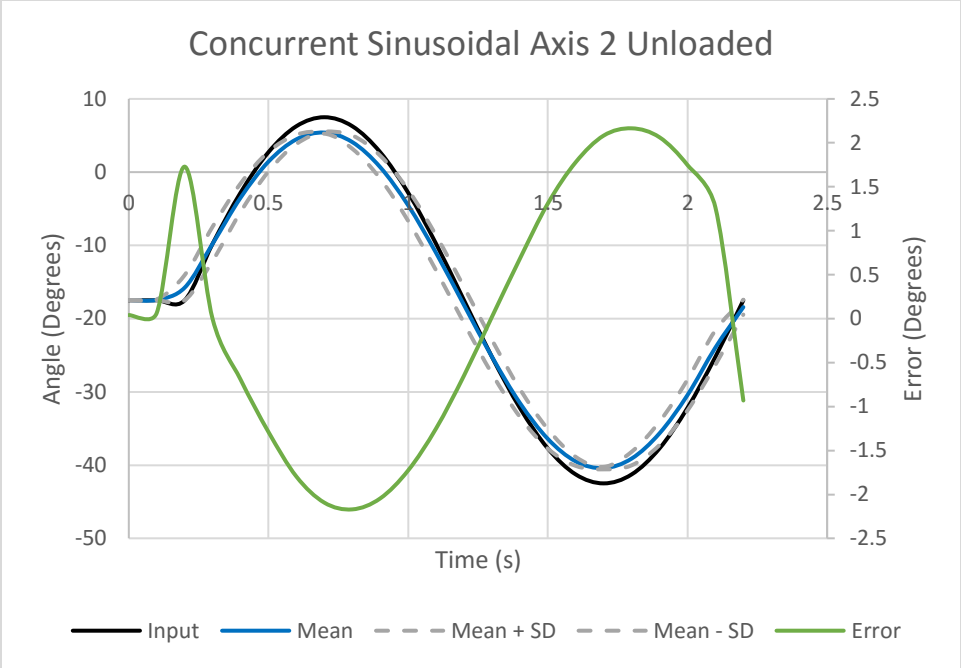

Figure 7: Accuracy and repeatability results for axis 2 of the JMR following concurrent sinusoidal wave input motion profiles without loading

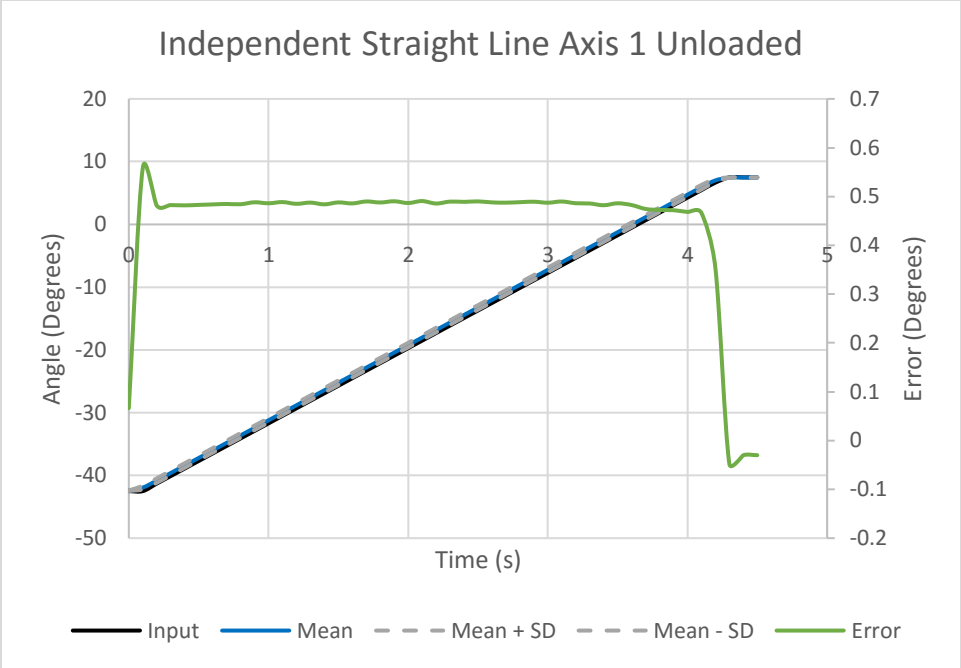

Figure 8: Accuracy and repeatability results for axis 1 of the JMR following an independent straight line input motion profile without loading

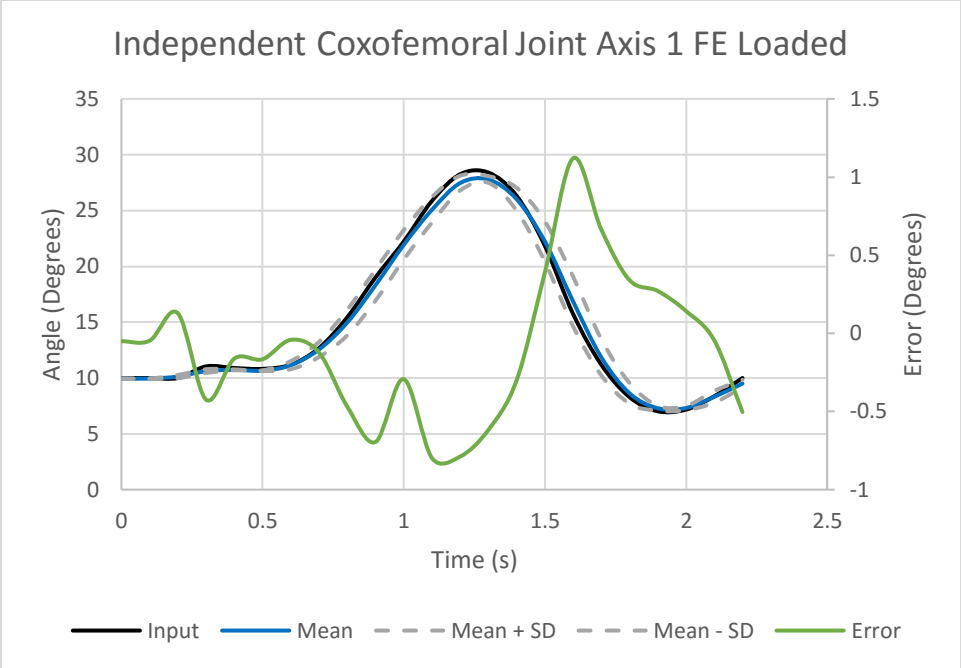

Figure 9: Accuracy and repeatability results for axis 1 of the JMR following an independent canine coxofemoral F/E input motion profile with loading

Table 2: Accuracy and repeatability results.

Error (Degrees)	Independent				Concurrent			
	Axis 1		Axis 2		Axis 1		Axis 2	
	Loaded	*Unloaded*	*Loaded*	*Unloaded*	*Loaded*	*Unloaded*	*Loaded*	*Unloaded*
Straight Line (max)	0.696	0.643	0.565	0.559	N/A	N/A	N/A	N/A
Straight Line (RMS)	0.598	0.563	0.522	0.462	N/A	N/A	N/A	N/A
Straight Line (ASD)	0.391	0.236	0.295	0.326	N/A	N/A	N/A	N/A
Sinusoidal Wave (max)	1.696	2.268	3.566	3.873	2.353	1.756	2.535	2.171
Sinusoidal Wave (RMS)	0.622	1.118	2.392	2.582	1.047	0.685	1.724	1.486
Sinusoidal Wave (ASD)	1.351	1.383	1.498	1.512	1.912	1.486	1.825	1.389
Canine Hip Motion (max)	1.120	1.051	0.451	0.824	0.671	0.762	0.340	0.294
Canine Hip Motion (RMS)	0.471	0.566	0.193	0.412	0.296	0.416	0.130	0.110
Canine Hip Motion (ASD)	0.708	0.550	0.222	0.190	0.517	0.380	0.165	0.136

Motion Profile Optimization

From the two curve-fitting algorithms tested, it was concluded the Cubic B Spline was more accurate as shown in Table 3.

Table 3: Curve fitting results for Cubic B and Catmull-Rom spline functions with higher accuracy performance bolded at each comparison

Error (Degrees)	*Type*	*Cubic B Spline*	*Catmull-Rom Spline*
Axis 1 Sinusoidal (max)	Independent	**2.268**	3.212
Axis 1 Sinusoidal (RMS)	Independent	**1.118**	1.907
Axis 1 Sinusoidal (ASD)	Independent	**1.383**	1.404
Axis 2 Straight Line (max)	Independent	0.559	**0.533**
Axis 2 Straight Line (RMS)	Independent	0.462	**0.451**
Axis 2 Straight Line (ASD)	Independent	0.326	**0.295**
Axis 1 Canine Hip Motion (max)	Concurrent	0.762	**0.651**
Axis 1 Canine Hip Motion (RMS)	Concurrent	0.416	**0.291**
Axis 1 Canine Hip Motion (ASD)	Concurrent	**0.380**	0.587
Axis 2 Canine Hip Motion (max)	Concurrent	**0.294**	0.304
Axis 2 Canine Hip Motion (RMS)	Concurrent	**0.110**	0.124
Axis 2 Canine Hip Motion (ASD)	Concurrent	**0.136**	0.212

Biomechanical Application Results

The JMR was effective in reproducing similar failure modes to those seen in vivo. An example of a failure method produced by the replicator is shown in Figure 10. The motion response with the cadaver in place was similar to the responses from the previous testing done in the accuracy and repeatability sections, but error data was not collected during this case study. This shows that the system can still operate effectively, even when the additional biological factors are considered.

Figure 10: TSC after testing

2.1.4 Discussion

Limitations

While the JMR is an affordable, multipurpose, modular dynamic motion replicator, some inherent drawbacks may be of concern. In the present configuration the system is designed

to replicate body weight distribution during the stance phase of the gait cycle. It does not replicate muscle forces. This can be important when simulating physiologic motions, because the muscle forces applied to the joint vary throughout motion profiles. Additionally, the replicator is currently set up to only test biaxial rotations. If triaxial motions of a joint are desired, an additional AOR will need to be included.

Future Work

The JMR has possible applications outside of testing canine coxofemoral joints. Due to their tri-axial nature, the JMR is ideal for testing joints. While it only has biaxial capabilities, the replicator is useful for simplified testing. Some examples of joints, which the JMR could replicate simplified motions, include the shoulder joint, the hip joint, and the ankle joint [16, 17].

While the JMR is designed for orthopedic applications, it could also be used to replicate other physiologic motions. Indeed, many physiologic systems that experience biaxial rotation could be tested utilizing the JMR. The JMR can be used to accurately replicate the biaxial rotation that occurs in vivo while maintaining relevant environmental conditions. This would require modifying or replacing the environmental chamber to secure the new physiologic system during testing. Due to the modularity of the replicator, this can be done by creating an enclosed mounting setup that follows the specifications outlined in the Fixture Attachment section. These modifications required would be more economic than purchasing a new replicator for testing.

The JMR is currently configured to perform testing on canine coxofemoral joints and the dead load rack system that is implemented on the device is optimized for such testing; however, the dead load rack can be easily adjusted to different heights to fit a wide range of specimens from different physiologic systems. In fact, if the protocol does not require the dead load rack, the system can be removed and replaced with a new custom system.

This simulation device can be upgraded by adding load cells and actuators. The device is currently limited to applying motion to the system, aside from a dead weight application. With the addition of actuators and load cells, dynamic loading could be applied to the system to more accurately replicate physiologic forces. Although these components are not currently a part of the replicator, the modularity of the device can easily allow for their addition.

A third AOR to replicate E/E would significantly upgrade the JMR's functionality. With all three axes of rotation, the JMR could fully represent the rotational capabilities of any physiologic system being studied. This could be done by adding a motor to the top of the JMR, or configuring the main frame to be able to rotate from the bottom. The ability to perform translational movements would also help the replicator more closely replicate physiologic motion. This could be performed by creating actuated tracks for the system to be able to move in each translational direction.

2.1.5 Conclusion

Through the testing, it is clear that the JMR is effective at modeling various physiologic systems. With the replicator's affordability, modularity, and multi-functionality, it is a valid alternative to many specialized systems. Rather than a machine that is purchased for the sole purpose of simulating one physiologic system, the JMR can be used for diverse applications, and can be reused for different projects, as well as modified to adapt to its purpose. The modular design of the system allows for easy modifications to improve the performance of the device. The simplicity of the original design allows for testing at different levels of sophistication, based on the desired precision.

2.2 Comparison of Three Modified Toggle Suture Constructs for Craniodorsal Hip Luxation in Dogs: An Ex Vivo Cyclical Biomechanical Study

2.2.1 Introduction

Hip luxation accounts for 90% of all traumatic joint luxations in dogs [17, 18]. While traumatic hip luxations are often treated initially with closed reduction, it is estimated that between 15 and 71% of cases experience re-luxation [19, 20]. Surgical treatment options for traumatic hip luxation include: open reduction, total hip replacement (THR), or excision arthroplasty such as femoral head ostectomy (FHO). A wide variety of surgical techniques have been described for open reduction of hip luxations including toggle suture construct (TSC) fixation [21, 22], ilioischial (DeVita) pin placement [23], Leeds transarticular pinning [24], extra-articular iliofemoral suture [25], triple pelvic osteotomy [26], and reconstruction of the ligament of the femoral head with the sacrotuberous

ligament [27] or a skin graft [28]. To date, none of these procedures are reported to be superior, with re-luxation rates ranging from 8.3-27% [17, 19-21, 25, 26, 29, 30].

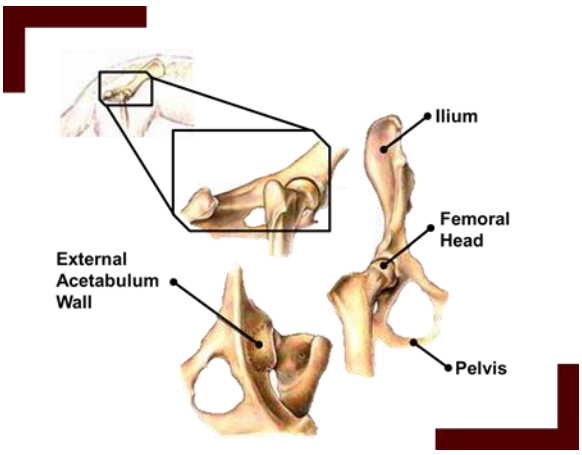

Figure 11: Coxofemoral joint consists of a ball (femoral head) and socket (acetabulum)

A variety of TSC fixations are commonly performed as open hip reduction procedures, as they are generally easy to perform and result in successful clinical outcome in many cases [17, 19-21, 25, 26, 29, 30]. While the suture and toggle maintain hip reduction during the early stages of healing, it has been suggested that long-term stability is provided by fibrosis of the traumatized joint capsule [31]. Thus, for TSCs to achieve a high level of clinical success, they must be able to maintain joint reduction without implant failure for several months after surgery. The original toggle fixation was reported by Knowles in 1953 [21]. Piermattei subsequently reported a modification of the Knowles technique, and this surgical technique became the gold standard TSC technique for nearly 40 years [32]. A number of clinical case series using the Piermattei technique, or variations thereof,

have subsequently been reported [21, 27-30, 33, 34]. Suture and toggle materials used in these case series included fascia lata, 80 pound monofilament nylon suture, No. 0 or No. 1 nylon suture material, #7 braided nylon, skin, sacrotuberous ligament, and #1 polypropylene suture paired with solid titanium rod toggle, toggle pin, bone biter suture anchor, stainless steel toggle rod, and k-wire. Toggle rod failure and re-luxation occurred in 8-21% of cases due to suture failure, suture loosening (stress relaxation), failure of the toggle, or a perceived pre-disposition to failure due to pre-existing hip dysplasia [20, 23, 29, 30].

To date, a modest number of biomechanical studies have been performed on toggle rod and suture constructs using fixed axis, single load to failure experimental designs [31, 35, 36]. In these ex vivo studies, the toggle rod construct failed by a variety of mechanisms, including: suture breakage, suture loosening, toggle failure, toggle pull out, femoral head fracture, and suture cutting through bone [31, 35]. Previously, mechanical performance of twelve TSC were evaluated for load to failure, mode of failure, and number of cycles to failure [36]. In this study, differences in systems were evident, as the type of toggle and suture material each affected biomechanical outcome measures. While the above studies highlight important biomechanical differences between commonly utilized toggle rod systems, fixed axis testing of components of the TSC system does not effectively represent the biomechanical environment of the post-operative canine hip. To the author's knowledge, biomechanical studies evaluating commonly utilized TSC systems using

cyclical testing protocols that allow dual axis gait analysis (replicated flexion/extension vs. abduction/adduction) have yet to be performed.

The goal of this study was to compare the biomechanical properties of three commonly utilized TSC fixation systems using a dual-axis, cyclical, ex vivo experimental design. Based on clinical experience and previously published work, we hypothesized that there would be significant differences in both the number of cycles to failure and mode of failure for three commonly utilized toggle rod systems. Additionally, we hypothesized that post-surgical toggle rod systems would more often fail during abduction/adduction as compared to the flexion/extension of the hip during replicated walk or trot.

2.2.2 Materials & Methods

Specimen Preparation

Twelve canine cadavers, euthanized for reasons unrelated to this study and weighing between 50-80 lbs. (22.7-36.3 kg, respectively), were acquired from a commercial vendor. Soft tissues were carefully dissected from the pelvis, sacrum, and femurs. Care was taken to ensure the hip joint capsules remained intact in order to preserve endogenous joint fluid and joint surfaces. Specimens were evaluated using ventrodorsal radiographs to screen for pre-existing conditions such as trauma, hip dysplasia, or open growth plates. Specimens with any radiographic abnormalities were excluded from the study.

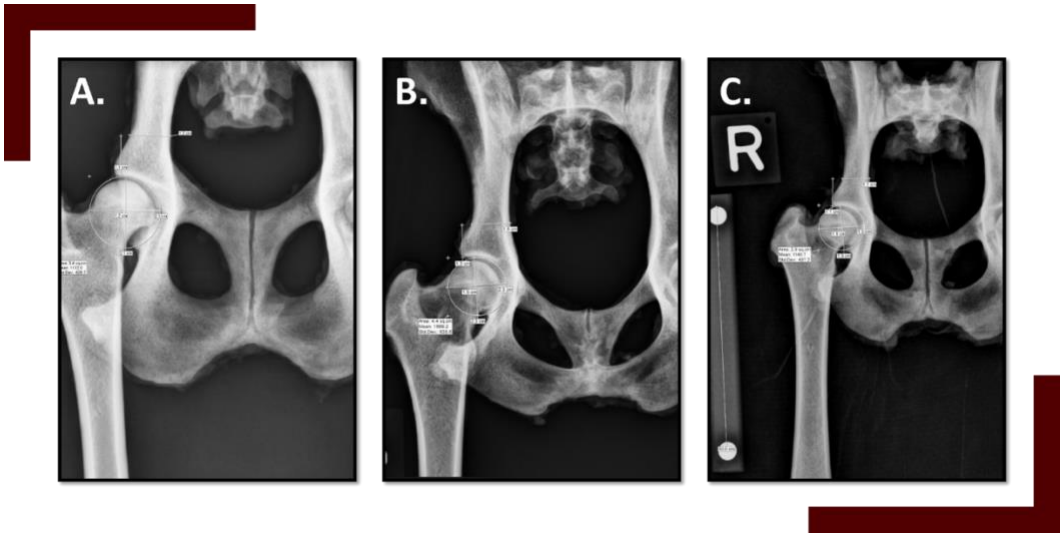

Figure 12: Three examples of specimen radiographs taken which later corresponded to A. Ethibond #04, B. Monofilament Nylon #05, and C. Tightrope #01

In addition, pre-operative radiographs were used to determine the anatomic position of each hip by measurement of the width of the ilium, maximum diameter of the obturator foramen, and position of the dorsal acetabular rim from the medial most aspect of the acetabular wall [Figure 13]. Hemipelvis specimens were created by transecting each cadaver on midline using a high-speed ban saw. Specimens were wrapped in saline-soaked towels, placed in plastic specimen bags, and frozen at -20°C.

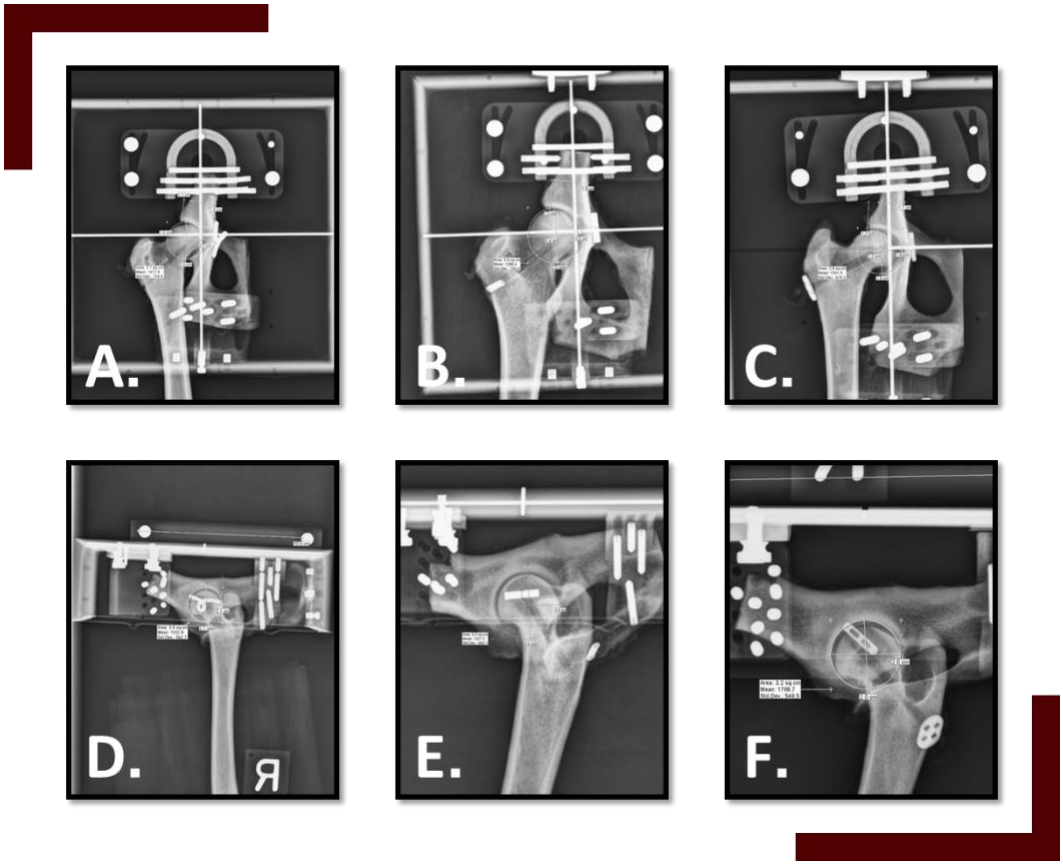

Figure 13: Three examples of specimen radiographs taken in lateral and ventral dorsal orientations while positioned within the environmental chamber. A./D. Ethibond #04, B./E. Monofilament Nylon #05, and C./F. Tightrope #01

Toggle Rod Fixation

Each specimen was brought to room temperature prior to toggle suture construct (TSC) fixation and biomechanical testing. The joint capsule was dissected free from each hip to replicate a maximally traumatized hip joint capsule and to eliminate soft tissue support in each cadaver. The round ligament was removed from the femoral head and acetabular

fossa. TSC fixation was performed using one of the following three fixation systems [Figure 14]:

1. monofilament nylon toggle consisting of a commercially available toggle rod (1/8" commercially available toggle, #001517, Securos Veterinary Orthopedics, Inc., Fiskdale, MA) and 80 lb monofilament nylon
2. Piermattei-#5 Ethibond toggle suture construct (TSC) consisting of a 3/32" diameter IM pin (#10332, IMEX Veterinary, Inc) fashioned into a toggle device combined with two strands of #5 Ethibond (Ethibond Excel Polyester Suture, Ethicon, Inc., Somerville, NJ) or
3. commercially available toggle system consisting of two titanium buttons and 2mm FiberTape (Footnote to TightRope™) (ArthrexVet, Naples, FL).

Each specimen was randomly assigned to a treatment group by randomization table.

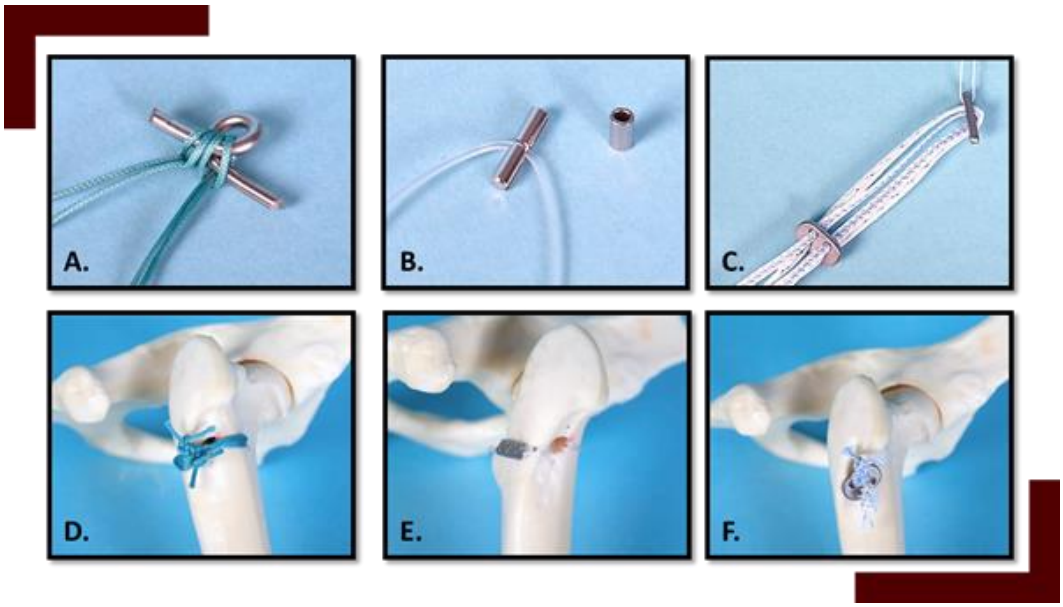

Figure 14: Piermattei toggle with #5 Ethibond suture (A. and D.), Securos toggle with 80 lb. monofilament nylon suture (B. and E.), and Tightrope stabilization system with FiberTape suture (C. and F.)

For all three stabilization systems, a drill hole was created in the medial acetabular wall, centered in the non-articular portion of the acetabular fossa. Acetabular hole size varied based on toggle rod diameter: monofilament nylon toggle (3.2 mm), Piermattei-#5 Ethibond TSC (6.35mm), dual button polyblend joint stabilization system (3.5 mm). For all treatment groups, a primary femoral bone tunnel was created using a combined aiming device and a 3.5 mm (commercially available toggle system), 3.2mm (monofilament nylon), or 2.7mm (Piermattei-#5 Ethibond TSC) drill bit using an "inside-out" technique. Drilling of the bone tunnel was initiated at the fovea capitis and proceeded laterally and distally to exit at the distolateral aspect of the greater trochanter). For the Piermattei-#5

Ethibond TSC, a secondary bone tunnel was generated in a craniocaudal direction using the 2.7 mm drill bit centered at the base of the intercondylar fossa, just proximal to the primary bone tunnel. A small Kirschner wire was placed in the primary tunnel during creation of this tunnel to ensure that the two bone tunnels did not intersect.

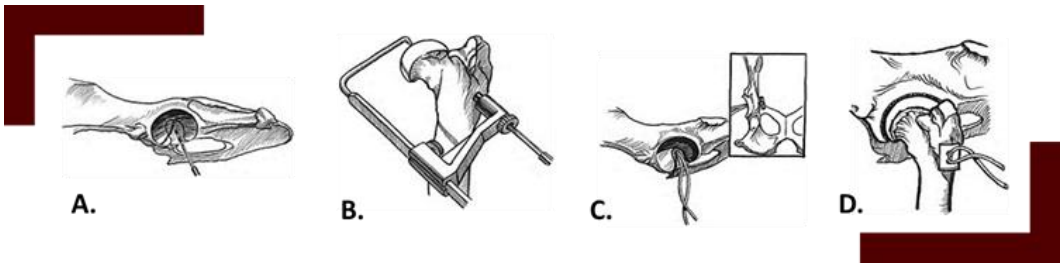

Figure 15: A. acetabulum hole drilling, B. femoral tunneling procedure, C. toggle rod/suture acetabular placement, and D. femoral threading of suture with tie off

For the monofilament nylon toggle system, the toggle rod and the associated strand of 80 lb. monofilament nylon leader line were inserted through the hole in the acetabulum. Tension was placed on the monofilament nylon to firmly seat the toggle rod to the medial aspect of the acetabulum. The two arms of nylon suture were fed through the primary bone tunnel from the fovea capitis to the distolateral greater trochanter. A suture passer was not used to pass the suture in order to prevent any mechanical weaknesses in the monofilament nylon suture caused by acute suture deformation. Each arm of the suture was passed through a commercially available polypropylene button (Polypropylene suture button, 55100S, IMEX Veterinary, Inc., Longview, TX) positioned at the primary bone tunnel exit hole on the distolateral trochanter as recommended by the manufacturer [37]. Manual

pressure was applied across the hip joint with the surgeon's thumb while slack was eliminated from the monofilament nylon. Visual inspection of the toggle on the medial aspect of the acetabulum was performed to ensure contact with the medial acetabular wall. While maintaining medial pressure on the greater trochanter, the monofilament nylon was secured with five throws based on surgical guidelines provided by the manufacturer [38].

For the Piermattei-#5 Ethibond TSC, two strands of #5 polyester suture were secured to hand-fashioned toggles using half-hitch knots around the converging arms of the toggle. The toggle was passed through the hole in the medial acetabular wall. The resulting four arms of suture were passed through the primary bone tunnel from the fovea capitis to the distolateral greater trochanter using a nitinol suture passer (ArthrexVet, Naples, FL). Next, two arms of suture were passed through the secondary bone tunnel from cranial to caudal using the suture passer. The remaining two arms were passed through the secondary bone tunnel in the opposite direction (caudal to cranial) using the suture passer. As with the monofilament nylon toggle, manual pressure was placed across the joint and slack eliminated by tensioning the suture at the exit point of the primary bone tunnel, then at each end of the secondary bone tunnel. Visual inspection was used to confirm that each toggle was in contact with the medial wall after removal of suture slack. While maintaining medial pressure on the trochanter, two arms of suture were tied on the lateral aspect of the greater trochanter and secured with five throws. The remaining two un-tied arms of suture were secured in an identical manner.

For the commercially available toggle system, the smaller of the two suture buttons and associated two strands of suture were inserted through the hole in the acetabulum and the suture button was firmly seated to the medial aspect of the acetabulum. The resulting four arms of suture were passed through the primary bone tunnel from the fovea capitis to the distolateral greater trochanter using the nitinol suture passer. The remaining four-hole button was threaded down to the lateral surface of the greater trochanter. As with the other techniques, manual pressure was placed across the joint and slack eliminated by manually tensioning the suture at the lateral aspect of the primary bone tunnel. Visual inspection was used to confirm that the suture button was in contact with the medial wall after removal of suture slack. While maintaining medial pressure across the joint, two arms of suture were tied over the four-hole button with four suture throws. The remaining un-tied arms of suture were secured in an identical manner. For all fixation systems and specimens, articular surfaces of the acetabulum and femoral head were regularly irrigated with 0.9% saline during implantation to prevent desiccation. Post-implantation radiographs were obtained to ensure proper toggle placement and to evaluate for technical errors. Specimens with improperly positioned bone tunnels or acetabular drill holes were excluded from further analysis.

Dual-Axis Cyclical Biomechanical Testing

Next, the distal aspect of each femur was removed with an oscillating saw just proximal to the femoral condyles in preparation for fixation to test fixtures. The approximate length, as measured from the greater trochanter to the location of distal aspect cut was 4.5” ±

0.25” (11.43 cm ± 0.635 cm). Additionally, the ilium wing was removed at the arcuate line, only to leave the body of the ilium. Removal of the ischial tuberosity and/or ischial arch were determined at the discretion of veterinary staff during mounting to test fixtures.

This prepared hemipelvis was mounted in a custom-designed poly [methyl methacrylate] (PMMA, a.k.a. acrylic) environmental chamber. The environmental chamber consisted of a body and top. The chamber body consists of a 5.75” x 5.75” x 2” radiolucent open-top box which allows for mounting of radiolucent ischium and ilium vises to secure each hemipelvis. In the floor-base of the chamber body, precision-ground (1/16” ±0.0005”) 303 stainless steel, radiopaque crosshairs were embedded to denote the central testing axis for flexion/extension and abduction/adduction gait cycles. In addition, the walls of the chamber body could be affixed with laser bore sights to denote the central axis of rotation in the vertical plane for both gait cycles. The custom, 3D-printed, poly [lactic acid] (PLA) ischium and illium vises of the chamber body contained adjustable 6-32 stainless steel, cone-point set-screws so that individual hemipelvis specimens could be secured. Ischium vises were also designed with 20° offsets to allow for accurate anatomical positioning; additionally, two sets of ischium vises were created for contralateral testing of both right- and left-sided cadavers. Through vise adjustment, the pelvis was moved in three-dimensions and secured in a position identical to the pre-operative radiographs while also being positioned so that the center of each acetabulum was positioned within the central axis of rotation in three-dimensions. Radiographs were obtained to verify appropriate anatomical position. This process was repeated until post-implantation positioning was

within 10% of pre-surgical measurements for the three metrics. The environmental chamber lid (which consists of a transparent, non-restrictive, non-pleated bellows and inlet/outlet ports for fluid circulation) were secured with a gasket to the chamber bottom. The distal end of the femur, along with the bellow's open end, was secured into a femoral pot, therefore creating a closed environment for the cadaver specimen.

Next, the environmental chamber was filled with a 0.9% saline solution. The cadaver-filled environmental chamber was mounted, via a couple of detent and plunger catches, into the Joint Motion Replicator (JMR) main body. The replicator is a dual-axis, closed-loop, coxofemoral ambulation system composed of two sub-systems. The first is a custom assembly consisting of two high-load 303 stainless steel yokes mounted to a frame of the same material type. The primary yoke emulates flexion-extension, while the secondary yoke emulates abduction-adduction. This subsystem mounts in series to the second subsystem, a dead-load rack system, which allows for loading onto the femur condyle to replicate resultant contact force magnitudes. Motion of the primary and secondary yokes is accomplished via two ST34-9e and ST34-3e high-torque stepper motors coupled to SMD-7620 independent drivers and PS-16 power supplies (National Instruments, Austin, Texas). Due to the complex nature of the motion profiles required, and need for future expansion, an NI cRIO-9076 integrated controller and chassis was chosen. This paired with the LabVIEW 2013 SP1 & NI SoftMotion control software (National Instruments, Austin, Texas) allows for highly configurable motion profiles such as coordinated and concurrent movements.

Once the mounting fixture was secured in the base platform, the line of sight laser lines was again used to confirm that the center of the acetabulum was coincident with the both central axis of rotation flexion/extension and abduction/adduction yokes. A "step-up" cyclical testing protocol was utilized, where specimens were cycled for 1,000 cycles in flexion/extension followed by 100 cycles of abduction/adduction. A table providing the number of cycles, joint range of motion, and applied load is provided [Table 4].

Table 4: Abbreviated cyclical testing protocol - this is an abbreviated form of the cyclical protocol used to test the TSC experiment groups, unlike the full tables which further breakdown the cycle sets in each phase by percent body weight and 1,000 flexion/extension (F/E) and 100 abduction/adduction (A/A) cycles

Test Phase	Load (% Body Weight)	F/E ROM (Degrees)	A/A ROM (Degrees)	F/E (Cycles)	A/A (Cycles)
Phase 1	0-65	40	35	13002	1302
Phase 2	0-65	55	50	12502	1252
Phase 3	0-65	65	60	12502	1252
			Total	38006	3806

Number of gait cycles and applied loads were determined based on pre-study pilot testing and approximated the number of gait cycles experienced by the post-surgical hip. This number was derived from the known number of gait cycles of a non-confined dog of 21,700 gait cycles per day [39]. We divided this value by two to account for one hemipelvis gait cycle occurring every other step. We further reduced this number of cycles fourfold to account for reduced number of gait cycles experienced by a leash-restricted

post-surgical dog. Calculating this number gives us an adjusted single-limb gait cycle count for a restricted-motion dog of 2,712.5 gait cycles per day; for this study 2,750 gait cycles is used as the daily metric. Selected loads were determined based on individual cadaver weight and the gait cycle under analysis. To replicate walking, 20% of body weight was applied to each specimen [40]. Next, 40% body weight was applied. Lastly, 65% of body weight was applied to the femur to replicate the trot [41].

Range of motion utilized for flexion/extension and abduction/adduction was based on prior reports in the literature as well as unpublished kinematic data from Labrador Retriever type dogs obtained in the institution's gait analysis laboratory.

To replicate hip range of motion at a walk (i.e. Phase 1), the hip was initially cycled from 7.5° of flexion to 32.5° of extension (40.0° range of motion) [16]. After completion of F/E cycle set, A/A cycles were initiated. To replicate hip range of motion during posturing to urinate/defecate, the hip joint was cycled from 0.0° adduction to 35.0° abduction (35.0° range of motion).

To replicate hip range of motion at a partial trot (i.e. Phase 2), the hip joint was cycled from 15.0° of flexion to 40.0° of extension (55.0° range of motion) [16]. To replicate an intermediate hip range of motion during posturing to urinate/defecate, the hip joint was cycled from 7.5° adduction to 42.5° abduction (50.0° range of motion).

To replicate hip range of motion at a full trot (i.e. Phase 3), the hip joint was cycled from 22.5° of flexion to 42.5° of extension (65.0° range of motion). To replicate fully advanced

hip range of motion during posturing to urinate/defecate, the hip joint was cycled from 12.5° adduction to 47.5° abduction (60.0° range of motion).

A complete testing protocol consisted of 38,006 F/E cycles and 3,600 A/A cycles which consisted of:

- parameter confirmation run: a single cycle set of two F/E and two A/A cycles was performed at the beginning of each phase of testing (i.e. Phase 1, 2, and 3) to confirm appropriate test parameters
- fixture settling run: a single cycle set of 500 F/E and 50 A/A cycles was performed during Phase 1 to allow for fixture and specimen conformity within the testbed; this was only performed in Phase 1
- no load run: a single cycle set of 500 F/E and 50 A/A cycles was performed during each phase of testing (i.e. Phase 1, 2, and 3)
- loaded run: multiple cycle sets (i.e. twelve) of 1,000 F/E and 100 A/A cycles were performed during each phase of testing (i.e. Phase 1, 2, and 3) with increasing levels of applied load (i.e. 20%, 40%, and 65% BW)

Run out was considered achieved at if: 1) a test sample completed the full testing protocol (i.e. cycles 38,006 F/E cycles and 3,806 A/A cycles), 2) the cross-head limit switch was tripped (i.e. sample luxation was much greater than clinical relevant), or 3) ultimate failure of TSC occurred. Testing was recorded with a video camera and failure mode was

determined by inspection during testing and evaluation of the video. Gait load, cycle number, and gait phase were collected at the time of failure for statistical comparison.

Specimens were loaded as described above until end of the testing protocol or toggle-rod failure occurred. Toggle rod failure was defined as biomechanical failure of the toggle rod/hip construct resulting in hip luxation. Upon hip luxation, the femur positioning arm of the ambulation replicator dropped toward the positioning arm baseplate, activating a cross-head limit switch that stopped cyclical testing and reported number of gait cycles at failure. Each test run was documented by video, and mode of failure, gait cycle at failure, anatomical angle at failure and number of cycles to failure was recorded by review of video, ambulation system software, and direct evaluation of the specimen at the time of failure. Post-failure radiographs were obtained of each specimen to evaluate the acetabulum and femur for changes not identified by visual inspection. Pre- and Post-images were compared to quantify shifting of the pelvic bone during testing (Figure 17). To quantify this potential motion, the width of the illium bridge was compared in the pre- and post-images. Multiple fixed objects, e.g. the clamp and retain bolt, were also analyzed to normalize any potential variations due to imaging technique between the pre- and post-images.

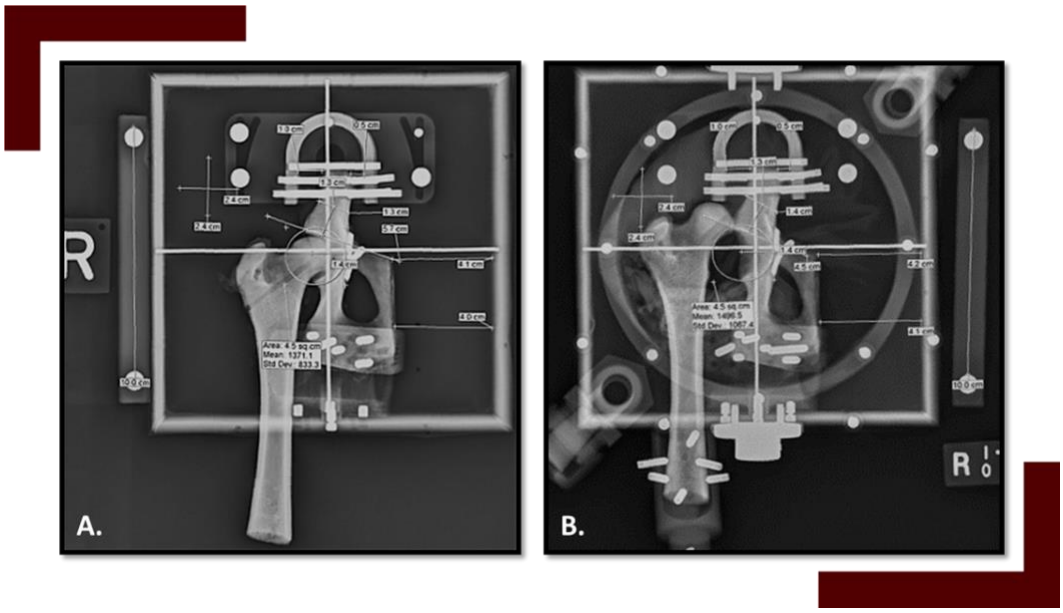

Figure 16: This figure depicts radiographs of cadavers mounted in the environmental pre- and post-testing, A. and B. respectively. After testing, the position of the pelvis is re-confirmed to ensure shifting has not occurred

Assessment of Subluxation During Testing

Prior to testing the system was moved to the home position with the specimen loaded and ready for testing to commence. A load equivalent to 65% BW was applied briefly to the specimen and then removed. The vertical displacement indicator was then set to zero as the initial condition. This effects a worse-case scenario for this measurement as the applied load will result some nominal vertical deflection without any appreciable subluxation. The vertical displacement was measured under load in the home position orientation every 1,100 cycles. Vertical displacement of the specimen in the testing system was used to develop a measure of hip subluxation during testing. The vertical displacement

measurement was used to calculate the translocation of the femoral head based on the assumption that the femoral head approximately followed a circular arc when displaced from the acetabulum [Figure 18A].

To develop the equations necessary to estimate the subluxation of the femoral head, we apply a constraint that limits motion of the distal end of the femur to a vertical line that passes through the center of the applied load and the center of the acetabulum (and coincidentally the femoral head when located firmly in the socket). The proximal end of the femur, specifically, the center of the femoral head is constrained to move along a circular arc with radius equal to that of the femoral head. Using a two-dimensional Cartesian coordinate system, wherein the origin is found by passing a line from the distal end of the femur through the center of the femoral head to the point on the pelvis where the femoral head makes initial contact [Figure 18A-18B], we can describe the location of the distal end of the femur and the center of the femoral head accordingly [Figures 18C-18D].

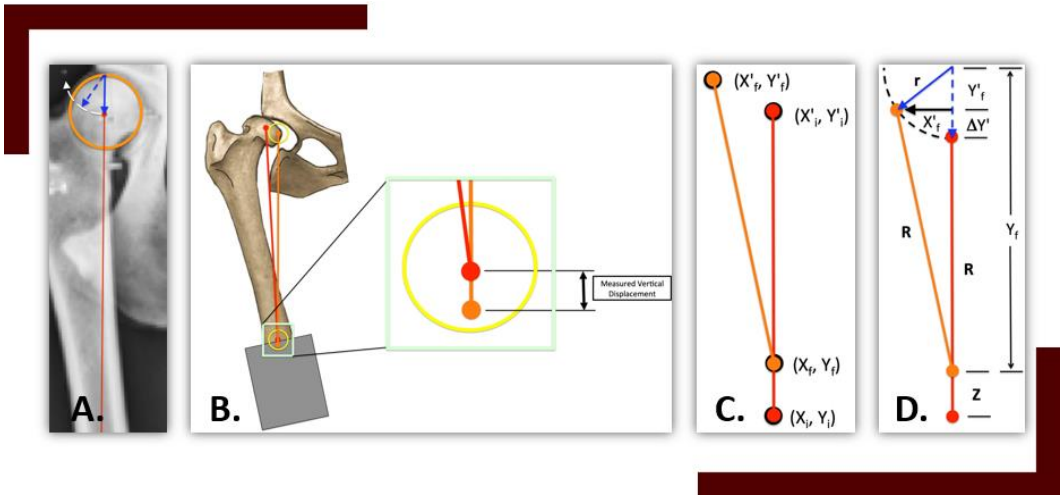

Figure 17: Equation development and graphical breakdown of dorsolateral displacement theorem

In Figure 17, A. The femoral head follows a circular path during subluxation as the load is applied. The vertical motion of the distal end of the femur is constrained along a vertical line passing through the center of the acetabular cavity, indicated by the red line. B. The red line extends from the distal end of the femur to the center of the femoral head in the initial state. The orange extends from the distal end of the femur to the center of the femoral head in the 'final' state. C. Coordinates of the points associated with the distal end of the femur and the center of the femoral head in the initial and final states. The origin of the coordinate system is found by passing a line from the distal end of the femur through the center of the femoral head to the point on the pelvis where the femoral head makes initial contact. This can be seen in D. The point from which the blue arrows emanate.

Initial Position

Distal end of the femur – (X_i, Y_i)

Center of the femoral head – (X_i', Y_i')

Current (or final) Position

Distal end of the femur – (X_f, Y_f)

Center of the femoral head – (X_f', Y_f')

The distance between the center of the femoral head and the distal end of the femur, $\boldsymbol{R}$, is constant i.e. there is no fracture or bending, and therefore the distance between the respective points on the specimen does not change when moving from the initial to current position:

$$(X_i - X_i')^2 + (Y_i - Y_i')^2 = \left(X_f - X_f'\right)^2 + \left(Y_f - Y_f'\right)^2 \qquad \textbf{Equation 1a}$$

Given the motion constraints at both ends of the specimen and that the radius of the arc of motion of the femoral head is equivalent to the radius of the head of the femur, $\boldsymbol{r}$, the choice of coordinate system leads immediately to:

$X_i = 0$

$X_i' = 0$

$Y_i = \boldsymbol{R} + \boldsymbol{r}$

$Y_i' = \boldsymbol{r}$

$X_f = 0$

Equation 1a simplifies to

$\boldsymbol{R}^2 = X_f'^2 + \left(Y_f - Y_f'\right)^2$ **Equation 1b**

Rearranging Equation 1b to solve for the horizontal displacement X'^2_f gives:

$X_f'^2 = \boldsymbol{R}^2 - \left(Y_f - Y_f'\right)^2$ where $Y_f = \boldsymbol{R + r - Z}$ **Equation 1c**

Note that Y_f is not measured directly. In Figure 18D, it can be seen that $Y_f = \boldsymbol{R + r - Z}$, where $\boldsymbol{Z}$ is the measured vertical displacement. For analytic expediency, we do not substitute for Y_f at this time. However, it is worth noting that $\boldsymbol{R}$, $\boldsymbol{r}$, and $\boldsymbol{Z}$, are all measured directly and therefore, Y_f is known quantity for the present purpose. Given that we have two unknowns, X'_f and Y'_f, another equation is needed.

Given that the arc of motion is approximated as circular, the second equation follows:

$Y_f' = \sqrt{\boldsymbol{r}^2 - X_f'^2}$ **Equation 2**

Substituting Equation 2 into Equation 1c gives:

$$X_f'^2 = \boldsymbol{R}^2 - \left(Y_f - \sqrt{\boldsymbol{r}^2 - X_f'^2}\right)^2$$

Solving for X'_f

$$X_f'^2 = \boldsymbol{R}^2 - \left(Y_f^{\,\boldsymbol{2}} - 2Y_f\sqrt{\boldsymbol{r}^2 - X_f'^2} + \boldsymbol{r}^2 - X_f'^2\right)$$

$$X_f'^2 = \boldsymbol{R}^2 - Y_f^{\,\boldsymbol{2}} + 2Y_f\sqrt{\boldsymbol{r}^2 - X_f'^2} - \boldsymbol{r}^2 + X_f'^2$$

$$2Y_f\sqrt{\boldsymbol{r}^2 - X_f'^2} = Y_f^{\,2} + \boldsymbol{r}^2 - \boldsymbol{R}^2$$

$$\sqrt{\boldsymbol{r}^2 - X_f'^2} = \frac{Y_f^{\,2} + \boldsymbol{r}^2 - \boldsymbol{R}^2}{2Y_f}$$

$$\boldsymbol{r}^2 - X_f'^2 = \left(\frac{Y_f^{\,2} + \boldsymbol{r}^2 - \boldsymbol{R}^2}{2Y_f}\right)^2$$

$$X_f'^2 = \boldsymbol{r}^2 - \left(\frac{Y_f^{\,2} + \boldsymbol{r}^2 - \boldsymbol{R}^2}{2Y_f}\right)^2$$

recall $Y_f = \boldsymbol{R + r - Z}$,

$$X_f'^2 = \boldsymbol{r}^2 - \left(\frac{(\boldsymbol{R} + \boldsymbol{r} - \boldsymbol{Z})^2 + \boldsymbol{r}^2 - \boldsymbol{R}^2}{2(\boldsymbol{R} + \boldsymbol{r} - \boldsymbol{Z})}\right)^2$$

And finally,

$$X_f' = \sqrt{\boldsymbol{r}^2 - \left(\frac{(\boldsymbol{R} + \boldsymbol{r} - \boldsymbol{Z})^2 + \boldsymbol{r}^2 - \boldsymbol{R}^2}{2(\boldsymbol{R} + \boldsymbol{r} - \boldsymbol{Z})}\right)^2}$$

This is the relationship that is sought. ***R, r,*** and ***Z***, are all measured directly and therefore known quantities. From this relationship, the horizontal displacement of the femoral head can be evaluated. Furthermore, given X'_f the vertical displacement can be determined by

$$Y_i' - Y_f' = \boldsymbol{r} - \sqrt{\boldsymbol{r}^2 - {X_f'}^2}$$

Finally, the total displacement, ***D***, is given by

$$\boldsymbol{D} = \sqrt{{X_f'}^2 + \left(Y_i' - Y_f'\right)^2}$$

Statistical Analysis

Descriptive statistics for continuous data (i.e. gait cycles to failure) as well as ordinal data (i.e. failure load, gait cycle failure, and failure mode) was generated. Data were reported as mean +/- standard deviation (SD) and compared using Student's t-tests with significance established at $P \leq 0.05$. Statistics were performed with Graph Pad Prism 7.0c (Graph Pad, La Jolla, CA) and Microsoft Excel 201 MSO 32-bit. In comparing the dorsal-lateral displacement data, the t-statistic was calculated using methods developed for unequal samples (device failures resulted in changing sample sizes as the protocol

progressed) and unequal variances. The Welch-Satterwaite equation was used to calculate the degrees of freedom for significance testing.

2.2.3 Results

Mean ± SD cumulative F/E and A/A cycle counts for TSCs were as follows: EB (32,901±9,417), MN (29,095±11,779), and TR (41,296±1,461). Both EB (P=0.0259) and MN (P=0.0115) underwent significantly fewer cumulative cycles at ultimate failure when compared to TR. Mean ± SD femoral head dorsal displacement were as follows: EB (13.95±6.38 mm), MN (7.24±4.78 mm), and TR (12.10±1.62 mm). While MN TSCs tended to experience the fewest cumulative gait cycles to failure, MN TSCs experienced lower displacement values as compared to EB (P=0.0321) or TR (P=0.0166). Considered together, these data suggest that if MN TSCs fail, failure more often occurs due to suture breakage as opposed to suture elongation.

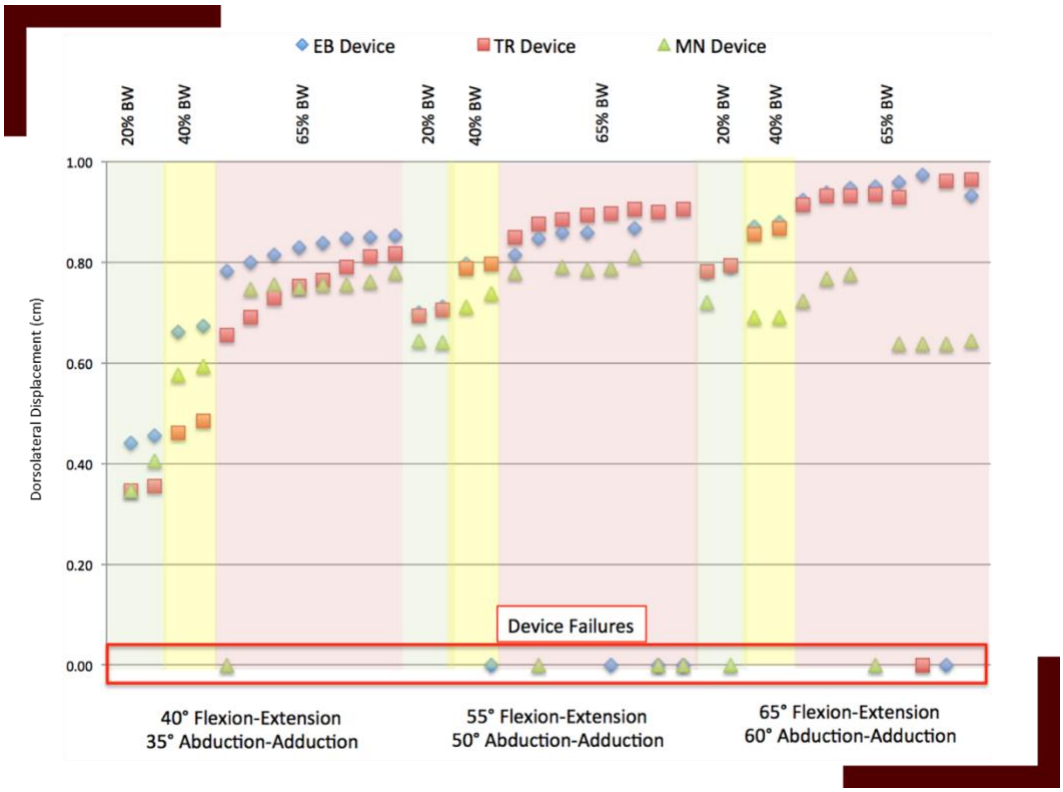

Figure 18: Average data map - here performance averages from all test runs have been plotted along the test regime cycle, at the graph bottom, devices that failed during testing are depicted

Figure 18 illustrates the average dorsal-lateral displacement data in centimeters collected for each device type at each time point through the entire study. As can be seen in this figure, three Flexion-Extension/Abduction-Adduction "phases" were tested at three different applied percent body weight (%BW) conditions. The range of motion was increased from 40% Flexion-Extension/35% Abduction-Adduction (Phase 1), to 55% Flexion-Extension/50% Abduction-Adduction (Phase 2), and then to 65% Flexion-Extension/60% Abduction-Adduction (Phase 3) for each sample. Within each Flexion-

Extension/Abduction-Adduction phase the %BW applied was increased from 20%BW (2000 cycles Flexion-Extension, 200 cycles Abduction-Adduction), to 40%BW (2000 cycles Flexion-Extension, 200 cycles Abduction-Adduction), and then to 65%BW (8000 cycles Flexion-Extension, 200 cycles Abduction-Adduction). Thus, each loading phase involved a total of 12000 cycles of Flexion-Extension, and 1200 cycles Abduction-Adduction. Each sample then was subjected to up to 36000 cycles of Flexion-Extension, and 3600 cycles Abduction-Adduction unless catastrophic failure occurred during testing.

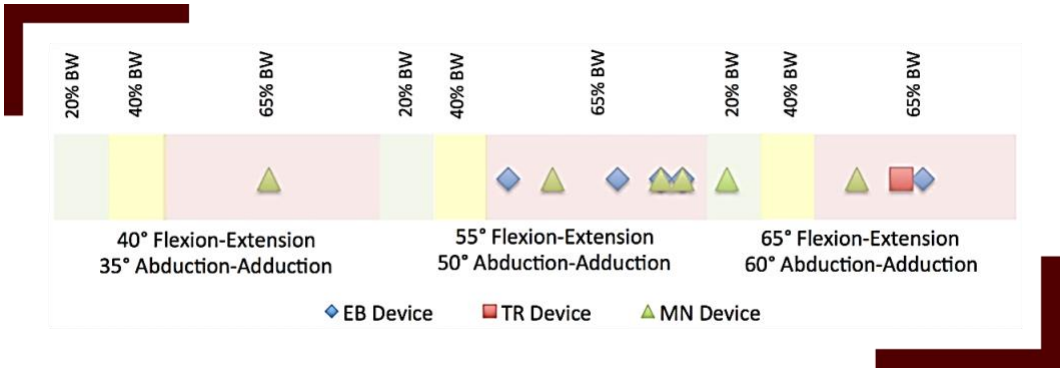

Figure 19: Failure timeline - this graph shows failed test groups as run through the various test regimes (i.e. body weight and range of motion). In Phase 1, 1 of 8 MN devices failed; during Phase 2 a total of 4 of the 8 MN devices failed, while 4 of the 8 EB devices also failed; and lastly during Phase 3 a total of 6 of the 8 MN devices failed, 5 of the 8 EB devices failed, and 1 of the 8 TR devices failed

In Figure 19, it can be seen that the TR devices outperformed the EB and MN devices with respect to resistance to catastrophic failure. Only one TR device failed catastrophically over the course of the study and this occurred in deep into Phase 3, i.e. under the most extreme conditions, 65% Flexion-Extension/60% Abduction-Adduction at 65%BW. Only

one device failed in Phase 1, an MN device that failed in 40% Flexion-Extension/35% Abduction-Adduction at 65%BW. Several MN and EB devices failed in Phase 2, 55% Flexion-Extension/50% Abduction-Adduction, at 65%BW. A total of 7 devices (3 MN, 4EB) failed under these conditions. An MN device subsequently failed early in Phase 3, 65% Flexion-Extension/60% Abduction-Adduction, at 20%BW. One of each device failed deep into Phase 3, 65% Flexion-Extension/60% Abduction-Adduction, at 65%BW. Figure 20 illustrates the device survival at each data collection point (1000 cycles Flexion-Extension, 100 cycles Abduction-Adduction) during the study. Here the attrition observed in Phase and the resistant to failure of the TR devices is readily apparent. Only 2 of the MN devices, and 3 of the EB devices, survived all three phases of the study protocol. Seven of the eight TR devices tested survived all three phases of the study.

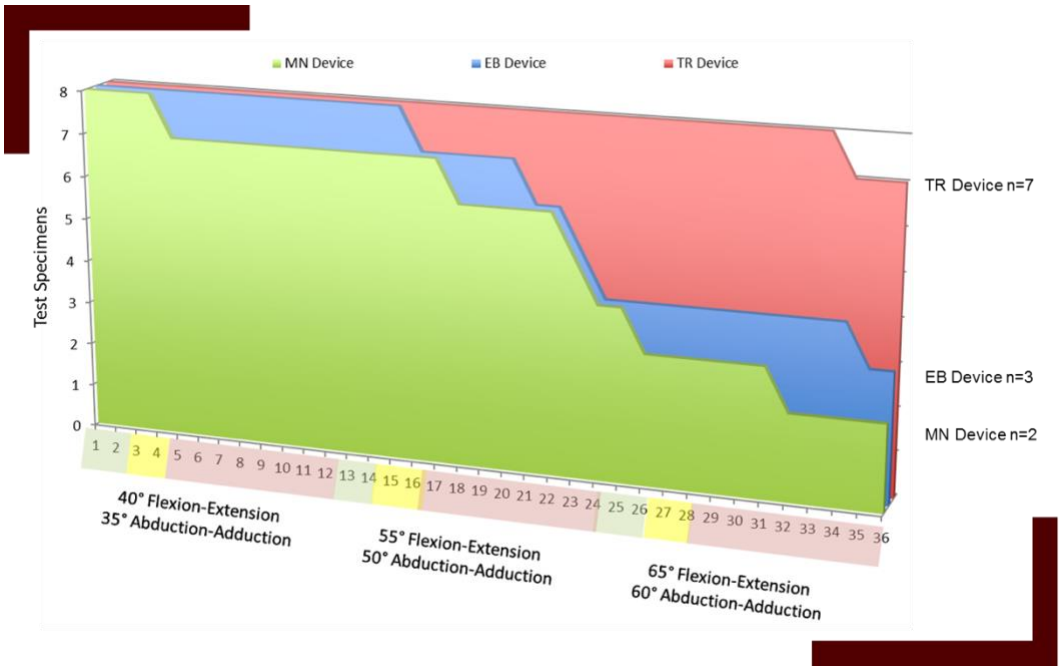

Figure 20: Failure structure of toggle suture constructs

Table 5 show the failure structure and modes of the TSC groups. When reviewing these graphical and tabular items together, 67% of specimen failure for MN devices can be attributed to suture failure, while EB devices have varied failure modes.

Table 5: Failure modes of TSC test specimens

	Suture Elongation	Suture Failure (Toggle)	Suture Failure (Femoral Head/Neck)	Femoral Head/Neck Bone Abrasion	Toggle Slipage	No Failure
Ethibond	0	1	2	1	1	3
Monofilament Nylon	0	4	1	1	0	2
Tightrope	0	0	0	1	0	7

As depicted in Table 6, ultimate failure counts were as follows: EB (5/8), MN (6/8), and TR (1/8). Of the combined 12 failures, 11 occurred during F/E motion while one occurred during A/A.

Table 6: Motion profile failure type

	Flexion/Extension Failure	Abduction/Adduction Failure	Total Failures
Ethibond	5	0	5
Monofilament Nylon	0	1	6
Tightrope	1	0	1

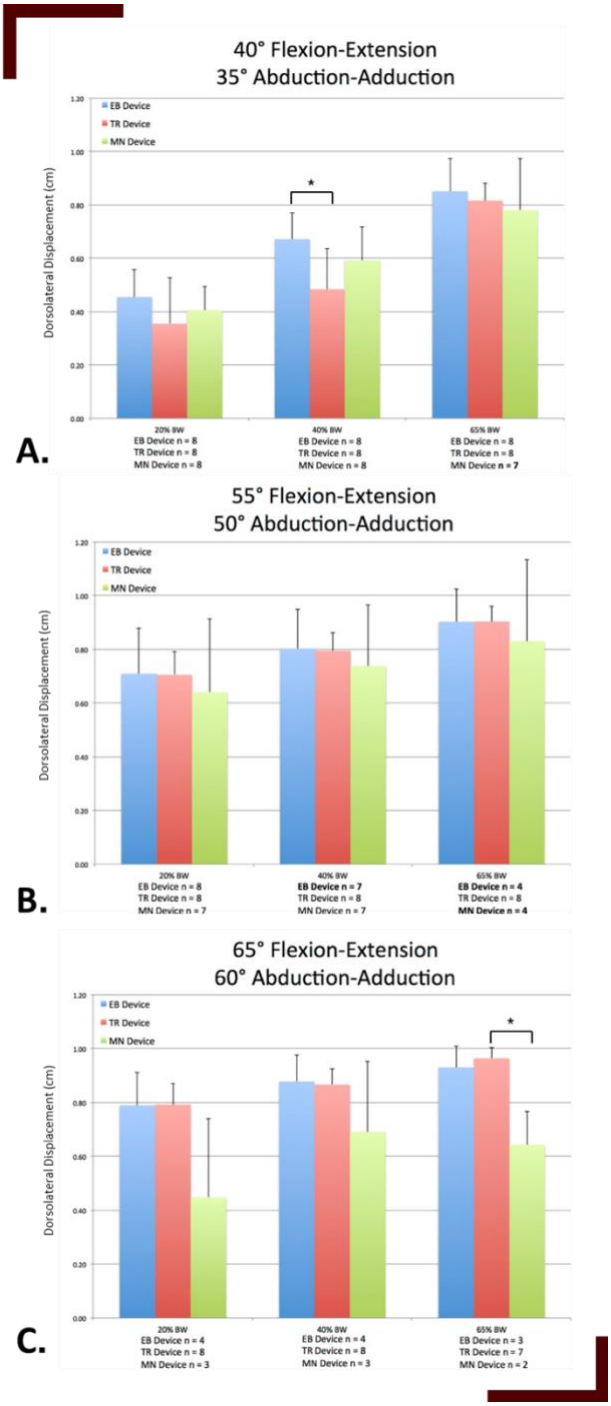

Figure 21: Dorsolateral displacement performance as a function of range of motion

In Figure 21 A-C, the average dorsal-lateral displacement measured at the end of each sub-phase (20%BW, 40%BW, and 65% BW) within each phase is plotted with the corresponding standard deviation. It can be seen that the TR devices performed more consistently than the EB and MN devices as evidenced by the smaller standard deviation observed in all but the first two Phase 1 (40% Flexion-Extension/35% Abduction-Adduction) sub-phases (20%BW and 40%BW). It is important to note the number of samples associated with each bar plot series, as failed devices resulted in important changes in those values as the study progressed. Thus, for example, in Phase 3 (65% Flexion-Extension/60% Abduction-Adduction), during the 20%BW sub-phase, it appears that the MN devices outperform the TR and EB devices. While strictly speaking this is true, by this point in the study only 3 MN devices remain. Finally, note that as the load is increased, the performance of the TR devices becomes more consistent, i.e. variance is reduced. Also note that caution must be used in drawing conclusions from changes in variance with the MN and EB devices as failures convolute the meaning of the changes in variance observed with those devices.

2.2.4 Discussion

In this study, TR consistently outperformed both EB and MN systems. TR resisted the greatest number of combined F/E and A/A cycles while also showing the least amount of variability across trials. EB TSCs performed on an intermediate level, with 4/8 constructs performing similar to TR. MN performance was unpredictable. While some MN

specimens completed the testing protocols, others experienced ultimate failure through suture breakage.

These results provide insight into the function of three common TSCs for hip luxation. Future work will focus on further improving cyclical gait modeling and the effect of ancillary support techniques on the function of TSC systems.

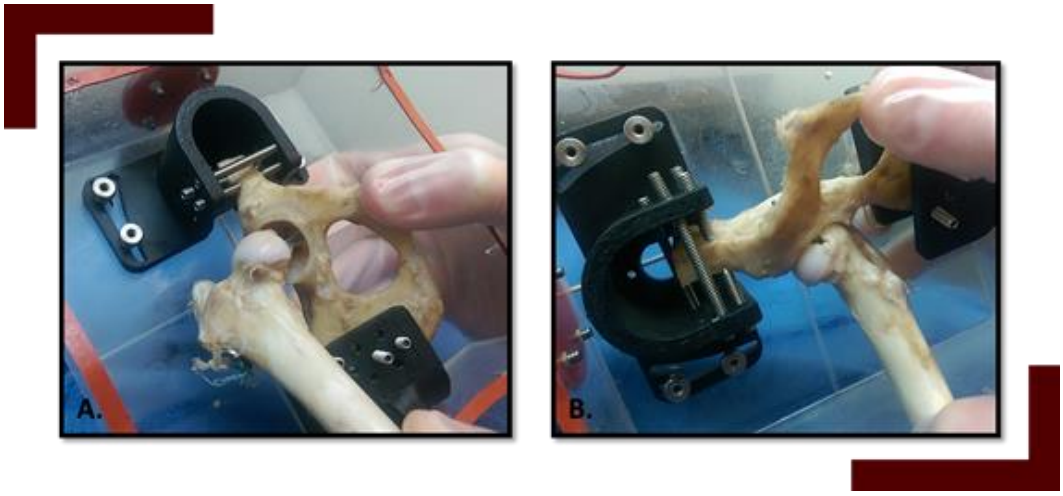

Figure 22: Views of Tightrope stabilization system post-experiment A. here we see some degree of luxation has occurred B. on the underside of the same specimen, we see a channel has formed due to repeated cyclical motion

2.2.5 Conclusion

Of the three commercially available implantable devices studied to treat the hip joint luxation injury in dogs, the Tightrope system provides the best barrier to re-luxation occurring by potentially providing the necessary time for natural fibrosis of the traumatized joint capsule to occur and, therefore, lead to long-term stability. The

Monofilament Nylon system proved to have unpredictable performance by having a wide variance in terms of cycles to failure and would not be recommended for use in treating hip luxations. Further in vivo studies would need to be done to further access the effectiveness of the Tightrope system and potential Ethibond variations.

3. HUMAN ORTHOPEDIC BIOMECHANICS

3.1 Development of an Environmental Chamber for Biosafety Level 2 Human Cadaver Testing

3.1.1 Introduction

Having the ability to apply load to a biological test specimen is important-but the ability to apply that load under appropriate environmental conditions while providing a level of security between experiment and operator is equally crucial. The simulation of physiologic environmental conditions is essential in cadaveric mechanical testing because their inclusion allows for a closer representation of the behavior of the biologic tissue in its natural environment. Such testing systems should include certain features to replicate physiologic conditions (e.g. temperature, loading range, humidity, etc.). Furthermore, a biological testing setup should always account for any blood borne considerations which may come into contact with the operator. For these reasons, and more, this work covers creation of an environmental chamber.

Environmental chambers are application-engineered for integration into load frames that are used for materials, component, and construct testing applications. These chambers must be designed so that they can accommodate a broad set of accessories including tensile grips, loading platens, measurement probes, etc.

It is the aim of this work to develop a chamber that: 1. could be used for a multiplicity of loaded testing applications and 2. implements safety features to minimize risk associated with running cadaveric tests.

3.1.2 Materials & Methods

Design Considerations

Several points were considered when designing this environmental chamber; they are as follows: temperature range, product in chamber, product load, construction, and biologic safety concerns.

One method for categorization of test chambers is the temperature range in which the chamber operates. The intent of this chamber is to be used for veterinary and human cadaveric testing; therefore, a nominal operating range of 37° C [98.6° F] ± 5° was set.

The product being tested in the chamber was also a major deliberation point for design of the environmental chamber. It is important to consider this factor early in the design phase; if all details (e.g. cadaveric tissue geometry, expectance of pathologies, desired mechanical test configurations, etc.) are not communicated, the resulting selection may not be best for the intended application and could cause safety risks. The chamber manufacturer should understand test objectives as well as possible. For cadaveric testing, the ability to submerge or maintain an equivalent tissue wet index comparable to the physiologic environment (e.g. 0.9% NaCl saline) is necessary.

Typically, the loading conditions the chamber needs to withstand is a primary design constraint of chamber manufacturing. To forecast the maximal loads, several common mechanical test setups can be considered (e.g. three-point bend, concentrically aligned compression, axially-offset extension, etc.) along with the most commonly used cross-head loads associated with bone testing [42]. In this case, both static and dynamic loads were considered. A maximum operating condition of 550 lbf [2000 N] was desired based on literature review, as it encompassed the majority of loads expected for use.

Construction of the chamber was a critical area of consideration. When considering various construction techniques, it is easy to believe they all accomplish the same objective equally. However, evaluating these details and choosing construction techniques can greatly affect the long-term reliability of the chamber. Seams for example can be chemically welded, heat molded, screwed, or snap riveted together; however, each of these methods has its own effect on seam strength. Seam strength is also related to fluid-tightness, and for design of this chamber, leakage caused by the pressure head due to a fully filled chamber was of concern. For development of this chamber, 75% of the total volume capacity is designated as the maximal operating capacity.

Biological safety was another concern for chamber creation. For example, servoelectric crosshead columns generally enter and exit a chamber through a topside opening. Generally, this is not a concern, but for cadaveric specimens, the risk of potential blood borne pathogens was considered. When discussing biological safety concerns, one

scenario considered was the potential for cadaver fluid splatter or aerosols development due to abrupt failure. For design of this chamber, methods to address blood borne splatter or aerosols was required. Clinical data, from previous research, revealed that 100µm ± 50µm was the nominal droplet diameter of aerosolized concern.

System Components

The chamber is an open-top rectangular prism made entirely out of poly [methyl methacrylate] (PMMA, a.k.a. acrylic). The main body (BB10, TestResources, Shakopee, Minnesota) is 12” [30.5 cm] in length, 10” [25.4 cm] in width, and 12” [30.5 cm] in depth. The temperature range in which the chamber can be controlled, via internal volume flooding, is between 15°C [59° F] to 45°C [113° F]. Test specimens can be placed entirely within the chamber via a horizontal breadboard (MB810U, Thorlabs Inc., Newton, New Jersey) mounted above the chamber floor. The breadboard footprint, 8" [20.3 cm] x 10" [25.4 cm], allows physical fixtures to be mounted via 1/4"-20 threaded features with 1” [2.5 cm] spacing. Although a multitude of additional fixtures could be used, (e.g. secondary 90° mounted vertical wall, pole-position frame) the initial test setup utilized three-pivot positioning arms, various locking fixtures, and a V-block for the first use of this system. The chamber is enclosed by a load-frame specific lid with a silicone o-ring and externally-mounted clasps. This lid’s function is: 1. minimize evaporation losses, 2. prevent transference of air borne contaminants, and 3. shield operators from potential flying hazards.

There are two aqueous delivery systems used within this embodiment of the testing chamber: 1. mist dispensing system and 2. flood-type fill/evacuation system. The mist dispensing system (100NF12, MSC Direct, Melville, NY) has a single outlet mist nozzle (5/16" nozzle, 5-1,000 µm @ 30-120 psi) with a 1 gal. [3.8 L] stainless steel tank. The flood-type fill/evacuation system is composed of a minimum of two 2.6 gal. [10 L] carboys (8-0402-13, Nalgene, Waltham, MA) with a heated recirculatory pump (210, PolyScience, Niles, IL).

Although not necessarily required for use, optical systems can be paired for use with the testing chamber. In the first experimental embodiment, a high definition camera (Vixia HF R600, Canon, Tokyo, Japan) was utilized along with a high-speed camera system (i-Speed, Olympus Corporation, Tokyo, Japan) and a LED lighting system (CN-160, Neewer, Guangdong, China). Additionally, a fully-submergible camera system (HX-A500, Panasonic, Osaka, Japan) has been suggested for in chamber video recording.

3.1.3 Results

As mentioned previously, a flood-type fill/evacuation system is integrated into the chamber body. Along with the ability to fully submerge the test product, this fill/evacuation system allows for the specimen to be heated. The working temperature range of the pump ranges from ambient to elevated temperatures, i.e. ~20° C [68° F] to 70° C [158° F] [43]. However, an optimal system temperature range of 25°C [59° F] to

45℃ [113° F] is recommended due to a relatively short ramp up time to equilibrium and the ability to maintain steady state temperature.

The flood-type fill/evacuation system also addresses physiologically relevant testing concerns since cadaveric bones are generally within a fluid envelope in situ. It is not always feasible to submerge a test setup; therefore, use of the mist dispensing system was also suggested as an alternative feature for maintaining a physiologically relevant wet index with cadaver test specimens.

The mist system also addressed biological safety concerns in the event that a cadaveric specimen catastrophically fails; thereby potentially releasing blood borne particles causing an airborne risk. It was key to estimate the droplet diameter size range which could occur during testing so an appropriate mist droplet diameter could be chosen.

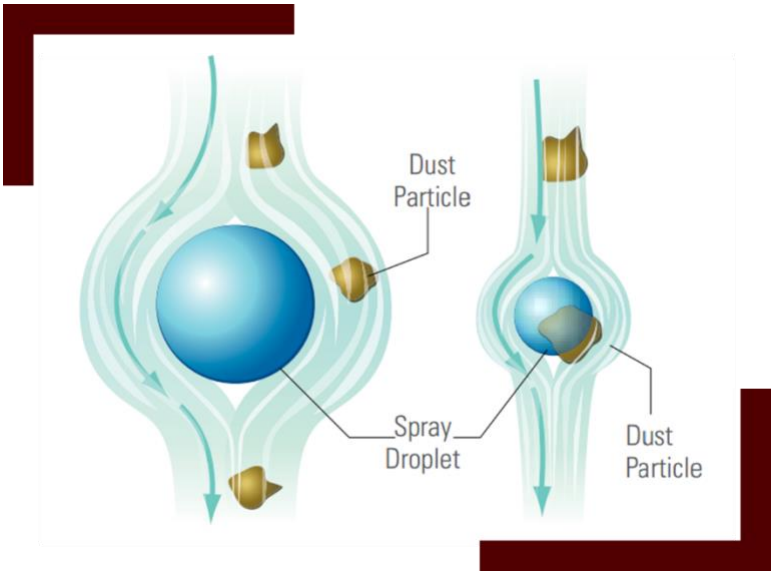

Figure 23: Mist droplet diameter capture

A beneficial feature of the system is that fluids moving into or out of the chamber do not need to be accessed during a specimen run: 2.6 gal. [10 L] carboys (8-0402-13, Nalgene, Waltham, MA) along with three multipurpose tank ports allow for free flow exchange.

3.1.4 Discussion

Testing chambers are application-engineered for integration into load frames that are used for materials, component, and construct testing applications. These chambers must be designed so that they can accommodate a broad set of accessories including tensile grips, loading platens, test fixtures, measurement probes, etc.

3.1.5 Conclusion

The climate chamber is a highly flexible system which allows for customization. Regarding future work, humidity control may be desired feature of future embodiments of the environmental chamber. The standard controllable range for temperature/humidity for most manufactures is 5-85° C [41-185° F] with 10-98% relative humidity (RH). Should a researcher decide to implement this feature, it becomes important for the individual to understand that relative humidity percentage is temperature specific. For example, the moisture amount in air at 10°C [50° F] and 50% RH is different at 60°C [140° F] and 50% RH. As air temperature is reduced, its ability to hold moisture is also reduced; therefore, for a given amount of water vapor in air-the lower the temperature, the higher RH. Figure 24

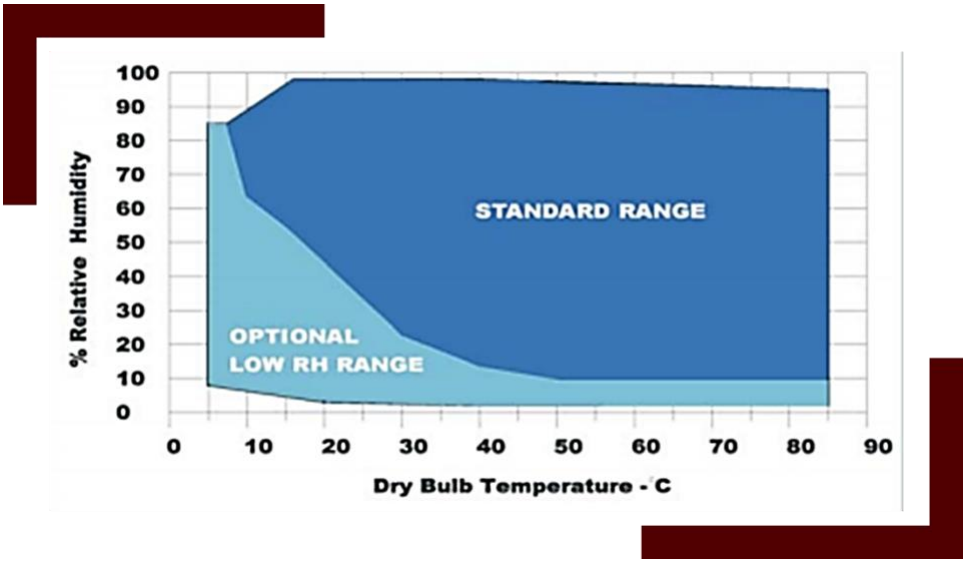

Figure 24: General humidity performance as a function of dry bulb temperature

Although there are multiple ways of implementing a humidity system in test chambers (e.g. water bath, boiler/steam generator, etc.), it is recommended to utilize the already existing mist system within the current embodiment of the test chamber. It is recommended that future researchers integrate a digital temperature/humidity sensor that feeds into a standard LabVIEW cRio controller with digital I/O module. Furthermore, this setup should include control of the air pressure regulator and fluid flow solenoid to the capacity tank of the mist system.

3.2 A Biomechanical Comparison of Fifth Metatarsal Fracture Fixation Methods- What is the Ideal Construct?

Fifth metatarsal base fractures of the metaphyseal-diaphyseal watershed junction are commonly treated with surgical fixation in athletes. Intramedullary screw fixation remains the most utilized construct, however plantar-lateral plating is an alternative to intramedullary screw fixation. The purpose of this investigation was to compare the mechanical strength of fracture fixation using an intramedullary screw versus plantar-lateral plating.

Twelve pairs of male cadaver feet (58 +/-7.5 years) were separated into two groups (plate or screw) to conduct contralateral comparative testing of two devices with equally numbered right and left feet in each group. For each fifth metatarsal, an osteotomy using a micro-sagittal saw was created 2.5 cm distal to the proximal tuberosity aimed for the articulation between the fourth and fifth metatarsals to replicate a Jones fracture. The plate

group underwent fixation with a 3.0mm four-hole low profile titanium plate placed plantar-laterally using three locking screws and one non-locking screw. The screw group underwent fixation with a 40 or 45mm X 5.5mm partially-threaded solid titanium intramedullary screw. The osteotomy and fixation were performed leaving all ligamentous and tendinous attachments in place to replicate a surgical procedure. After fixation, the metatarsals were excised for biomechanical testing. Cyclic cantilever failure testing was conducted using a gradient-cycle method (force applied at gradually increasing loads). Sinusoidal loading forces at a constant frequency of 0.25Hz were applied to the metatarsal increasing by 5.0 pound-force (lbf) increments per 10 cycles. Testing was concluded once each specimen had experienced mechanical failure of the implant or bone. Failure mode, number of cycles to failure (CTF), peak failure load (PFL), gap width (GW) at the last mutual pre-failure loading, and video data were recorded. The paired two-tailed t-test (α=0.05) was used to compare the two groups with a $P<0.05$ set for significance.

Failure mode in both groups occurred predominantly at the bone-implant interface. There was a significant difference found between the plate and screw groups with regard to CTF (63.9 vs 37.3 P=0.01), PFL (35.8 lbf vs 21.7 lbf, P=0.01), and GW (0.0mm vs 3.2mm, $P<0.01$) respectively reported as means.

This biomechanical investigation demonstrated plantar-lateral plating is significantly stronger than an intramedullary screw for Jones fracture fixation. Larger CTF and PFL along with smaller GW were recognized in the plate group compared to the screw group.

3.2.1 Introduction

Bone healing occurs by one of two different repair mechanisms: primary bone healing and secondary bone healing. The degree of fracture reduction, the effect of the implant on the strain at the fracture site, and the biological environment of the fracture determine whether a fractured bone heals through primary or secondary bone healing. Primary bone healing, also referred to as direct bone healing or primary osteonal reconstruction, occurs under conditions of absolute stability in which strain at the fracture has been functionally eliminated by treatment of the fracture with anatomic reconstruction, compression of bone fragments, and rigid fixation of the bone column. Due to the fact that anatomic reconstruction and rigid fixation are necessary, primary bone healing only occurs if fractures are stabilized using certain surgical techniques. Examples include lag screw fixation with or without an associated neutralization plate, cerclage wire in conjunction with a neutralization plate, and application of a dynamic compression plate. When fractures are surgically stabilized with anatomic reconstruction and rigid internal fixation, the strain at the fracture site is eliminated, and the injured cortex restores continuity across the fracture by the direct deposition of new bone. This occurs through the process of intramembranous ossification in which surviving osteoblasts and osteoblast precursors directly deposit bone at the fracture. Although in theory it is possible to reconstruct the bone column with anatomic reconstruction and rigid internal fixation (resulting in absolute stability around the entire circumference of bone), in reality there is never complete

congruence of the entire bone surface. For this reason, primary bone healing always occurs through a combination of both contact and gap healing.

Contact healing occurs when the distance between bone ends is less than 0.01 mm and interfragmentary strain is functionally eliminated (<2% strain). In this case, primary osteonal recontstruction occurs. This process involves the elongation of longitudinally oriented osteons to directly bridge the fracture. “Cutting cones” of osteoclasts form at the ends of injured osteons adjacent to the fracture. Osteoclasts form a spearhead at the apex of each cutting cone and advance across the fracture, removing dead bone in their path. As each cutting cone crosses the fracture, an organized group of osteoblasts at the tail end of the cutting cone deposit new bone, resulting in the simultaneous resorption and formation of bone. The orientation of these osteoblasts, along with the longitudinal elongation of multiple cutting cones from adjacent osteons, results in the deposition of lamellar bone across the fracture. Gap healing, on the other hand, occurs in the small gaps between zones of contact healing. Although the bone is technically not in direct apposition, absolute stability is provided by the contact zones on either side of the gap. Interfragmentary strain is functionally eliminated, and the gap width must not exceed approximately 1 mm for gap healing to occur. The small gap is initially filled with a fibrin matrix and vascular sprouts that develop via angiogenesis. The provisional wound matrix is rapidly remodeled with collagen type I, type III, and other extracellular matrix components associated with bone formation. Within days to weeks, lamellar bone fills the gap in a process that mimics intramembranous ossification.

Fractures that are not anatomically reconstructed and stabilized with rigid internal fixation heal by an organized process known as secondary bone healing, also referred to as indirect bone healing. Interlocking nails, bridge or lengthening plates, and plate/rod fixation, when used to bridge large zones of comminution, provide relative stability and result in secondary bone healing. Secondary bone healing is an organized series of five overlapping, yet unique, phases: inflammation, intramembranous ossification, soft callus formation (chondrogenesis), hard callus formation (endochondral ossification), and bone remodeling.

Fifth metatarsal base fractures occurring at the metaphyseal-diaphyseal junction can present a difficult clinical problem, especially in athletes who desire an early return to competition. This acute fracture, commonly referred to as the "Jones Fracture" was first described by Sir Robert Jones in 1902 and is located approximately 1.5-3.0cm distal to the tuberosity in an anatomic watershed area that experiences repetitive stresses during any weight bearing activity [44, 45]. This relatively hypovascualar environment located at the metaphysical-diaphyseal junction is a consequence of the intramedullary nutrient artery to the fifth metatarsal entering in the medial middle third of the diaphysis and supplying only small vessel retrograde flow to the proximal fifth metatarsal which is disrupted in a Jones fracture [44]. For these reasons, the fracture can be at risk for delayed union up to 67%, and nonunion up to 28% when treated non-operatively [46-50]. The fracture often results from a forced inversion of the foot at which time the foot is usually plantarflexed and the

distal aspect of the fifth metatarsal is adducted while the strong intermetatarsal ligaments hold the proximal aspect of the metatarsal in place [44].

Operative fixation of the fracture is recommended for athletes, and can decrease the delayed union and nonunion rate associated with these fractures [49, 51-53]. A common fracture fixation technique is intramedullary screw fixation [48, 49, 52-55]. However, even after intramedullary screw fixation and successful fracture reduction; patients can still experience delayed unions up to 27%, nonunions up to 9%, and even refractures up to 7.3% [46, 47, 50, 52, 56-58]. Larsen, et al showed a significantly higher proportion of fixation failures occurring in athletes compared to other patients reporting a 40% failure rate with all but one occurring in an elite athlete ($P<0.01$) [59]. The same study recognized that on average, athletes declared themselves asymptomatic three weeks prior to other patients, which frequently led to increased early activity [59]. Failed intramedullary screw fixation often requires revision surgery consisting of bone grafting at the fracture, and either repeat intramedullary screw placement or plate fixation [54, 60]. Plate fixation in the past has been difficult in this area due to hardware prominence and poor bone quality, however, Choi reported on 17 patients treated with hook plate fixation with only one requiring hardware removal due to prominence [61]. Furthermore, the introduction of low profile locking plates reduces the hardware profile even more. The purpose of this investigation was to compare the mechanical strength of fracture fixation using an intramedullary screw versus plantar-lateral plating. The hypothesis is that a Jones Fracture

fixation method incorporating a plantar lateral plate will provide a more biomechanically stable construct than an intramedullary screw.

3.2.2 Materials & Methods

Specimen Preparation & Fracture Model

Twelve matched pairs of male cadaver feet were purchased from the Research for Life organization for this contralateral biomechanics study. Each pair was harvested from the same donor and labeled accordingly. In addition to an arbitrary numeric identifier, the feet were labeled with the letter "R" or "L" designating right or left, respectively. Mean donor age was 58 +/-7.5 years old.

A fracture simulating osteotomy was performed at the fifth metatarsal approximately 2.5 cm distal to the tip of the proximal tuberosity. This procedure was performed under fluoroscopic visualization with a micro-sagittal saw targeting the mid-aspect of the articulation between the fourth and fifth metatarsal by an orthopedic surgery sports medicine fellow supervised by a foot and ankle fellowship-trained board certified orthopedic surgeon with 19 years of experience. The osteotomy was performed leaving all ligamentous and tendinous attachments intact and was brought through both the near and far cortices to establish a complete unstable fracture situation. Therefore, the surgical repair procedure was an accurate simulation of the process required for device placement. Upon completion of the osteotomy procedures on a matched pair, one metatarsal was assigned to the screw group while the other was assigned to the plate group. Following

the respective fracture fixation procedure, the treated fifth metatarsal was separated from the foot and prepared for in vitro mechanical testing of the bone-device construct. A total of twelve specimens were assigned to each treatment group for biomechanical testing. The same surgical team performed all osteotomy and fracture fixation procedures.

Plate Application

The skin was incised to expose the tuberosity and the shaft of the metatarsal to allow for the osteotomy and plate application [Figure 25].

Figure 25: Incision for osteotomy and hardware placement

A low profile straight, 4-hole, titanium, 3.0mm plate (AR-8952TS-04, Arthrex, Inc. Naples, FL) was contoured to fit the plantar-lateral aspect of the fifth metatarsal prior to osteotomy [Figure 26]. After the osteotomy, the contoured plate was positioned, across the fracture site, such that two locking holes were aligned on the proximal side; the oblong and remaining locking hole were aligned on the distal side of the defect.

Figure 26: Low profile locking plate and solid partially threaded screw

A hole was drilled bicortically with the 2.2mm drill bit using the locking tower guide through the proximal locking hole closest to the fracture. An appropriate length 3.0mm cortical screw was placed in order to effectively reduce the plate to the bone. This process was repeated and another appropriately-sized cortical screw was placed eccentrically (i.e. distally-situated) in the oblong hole to allow for the dynamic compression required to reduce the fracture. The most proximal hole was then drilled with the locking tower guide in place and a 3.0mm locking screw was placed. Care was taken to avoid violation of the metatarsocuboid joint or the articulation between the fourth and fifth metatarsal. The remaining distal hole was drilled using the locking tower guide and a locking screw was placed. Finally, the initial cortical screw that was placed was removed and replaced with a locking screw. Therefore, the final repair incorporated a plate construct with three locking screws and one cortical screw, strategically placed to effectively reduce the fracture area [Figure 27].

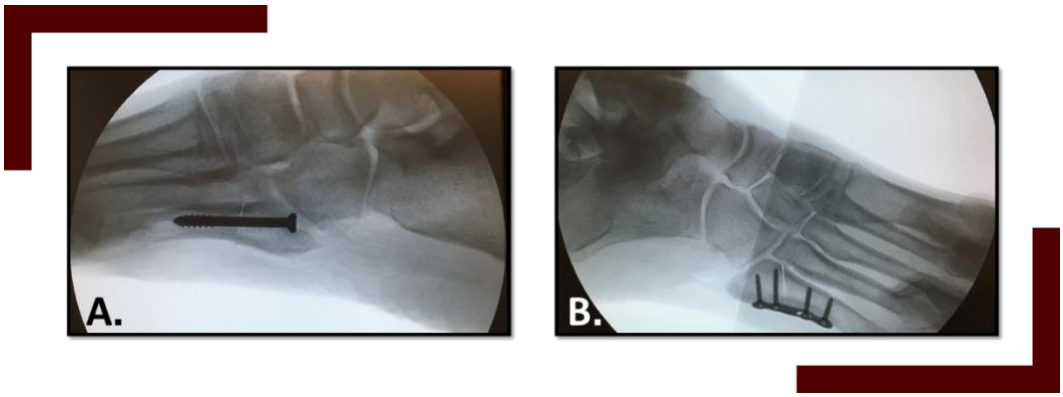

Figure 27: Plantar lateral plating (a) and intramedullary screw (b)

Intramedullary Screw Application

The skin was incised to expose the tuberosity and the shaft of the metatarsal to allow for the osteotomy and the screw to be placed [Figure 25]. The starting point for the screw insertion was just medial to the insertion fibers of the peroneus brevis, approximately 5.0mm medial and 10.0mm dorsal to the palpable aspect of the tuberosity, thereby avoiding branches of the sural nerve [62]. A drill guide was used to insert a guide-pin down the shaft of the fifth metatarsal at an angle approximately 7.0^0 from cranial to caudal relative to the sole of the foot [62, 63]. This was performed with fluoroscopic guidance to continuously check the anterior-posterior, lateral, and oblique views to ensure appropriate placement within the intramedullary canal. Once the guide-pin was advanced past the fracture line, 4.0mm cannulated drill bit was introduced over the guide-pin, drilling to a depth of approximately 40.0-45.0mm under fluoroscopic guidance depending on the

length of the cadaveric fifth metatarsal. Special care was taken to avoid penetration of the distal fifth metatarsal cortex.

A 5.5mm cannulated bone tap (AR-8956C-55T, Arthrex, Inc., Naples, FL) was then introduced over the guide-pin to the same depth. A 40.0mm or 45.0mm X 5.5mm titanium partially threaded solid screw (AR-9055-40PT, AR-9055-45PT, Arthrex, Inc., Naples, Florida) was then placed using fluoroscopy to ensure that all the screw threads would be located distal to the fracture location [Figure 26].

The appropriate screw was chosen based on fluoroscopy findings and was then placed while the fracture was held reduced [Figure 27].

Biomechanical Testing

The mechanical performance, of the implantable fracture fixation devices, was evaluated using a cantilever bend test protocol. While the in vivo loading conditions on the fifth metatarsal are complex, this mode of testing was chosen as a worst case scenario from a purely mechanical perspective, i.e. this loading condition represents application of the resultant force in a manner that is most likely to produce the gap recurrence failures observed in the clinical setting.

From Queen et al. 2007, it was found that the force experienced in the lateral forefoot for side- and cross-cut actions were 45 and 210 lbf, respectively. Since these two motions both predominately place reaction forces onto the fifth metatarsal in the lateral-to-medial

loading direction, these forces, along with the pilot results, were used as the basis for establishing load protocols.

Due to the absence of all soft tissue, litigious connections and footwear support, it was decide that target loading regime would operate on the lowest performance region. Furthermore, increments of ~10% (i.e. 5 lbf) were implemented to capture the performance capability prior to failure. This step resolution was confirmed to be adequate in pilot testing.

Following the osteotomy and fixation procedures, the bone-device construct was separated from the foot and soft tissue attachments. The specimens were then potted in clear, 25.4mm ID, acrylic tubes using a poly [methyl methacrylate] fill material (0921386 Keystone Bosworth Fastray Set, Bosworth Company, Skokie, Illinois). Prior to potting, a 25.4mm x 18-gauge brad nail was transversely embedded into the proximal end of the pot and metatarsal to provide greater affixation within the pot [64-66]. The nail was positioned so that its placement would not hinder the pot fixation screws from acquiring full purchase directly onto the bone surface. Additionally, the ends of each metatarsal were wiped down with acetone to dry out tissue and breakdown fats at a superficial level in preparation for potting [64-66].

Care was taken while potting the specimens to avoid adhesive contact with the orthopedic hardware as well as the fracture site. This was accomplished by covering the head of the intramedullary screw as well as the proximal end of the plate construct with modeling clay

prior to potting. Otherwise the hardware would have come into contact with the epoxy [64, 66, 67]. A custom-designed jig was used during the potting process in order to properly align the proximal and distal acrylic pots [Figure 28].

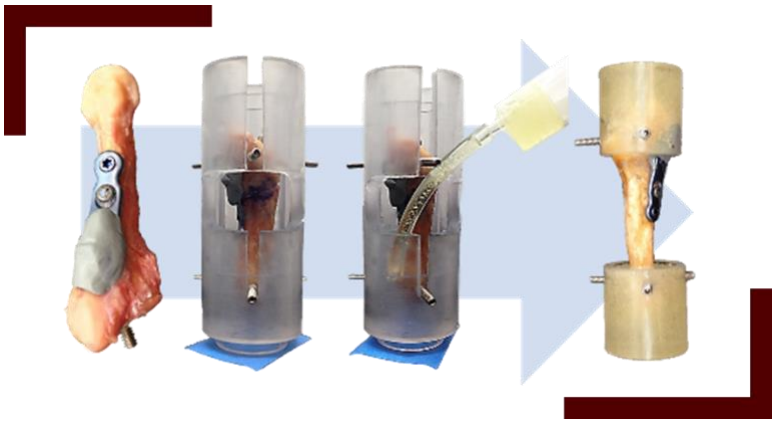

Figure 28: Stages of fifth metatarsal potting process. From left to right, first image depicts the set screw and modeling clay on the specimen. Second image shows alignment of the specimen in the acrylic jig. The third image demonstrates addition of epoxy. Finally, the fourth image depicts the final potted specimen.

After 24 hours, (much greater than the manufacturer-specified five-minute set time), the pot holding the distal aspect of the metatarsal was drilled to have a 12.7mm diameter hole positioned in such a way to allow for medial-lateral loading. The effective lever arm spanning the distance from the fixation hole center and the replicated fracture location was recorded for each metatarsal. During the curing process the test specimens were wrapped in a saline soaked towel to prevent drying.

The proximal end of the potted metatarsal was fixed in a V-block, which was mounted to a ThorLabs breadboard integrated within a modified environmental chamber (BB10,

TestResources, Shakopee, Minnesota). The distal end was then connected to a dual-column load frame (830AT, TestResources, Shakopee, Minnesota) via a custom-designed loading fixture fitted with a clevis pin assembled transversely into the distal pot [Figure 29]. A fatigue-rated web shear load cell (F250, TestResources, Shakopee, MN) with a maximum fatigue rating of 250 lbf [1.1kN] and 0.2% resolution was chosen to capture the expected performance range of the constructs derived from previous studies [64, 65, 68].

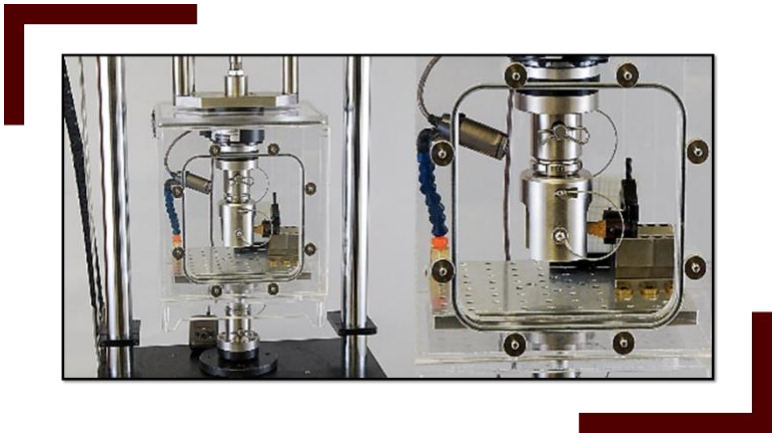

Figure 29: Testing chamber and fixture pilot setup with a 3D printed metatarsal environmental chamber with the integrated ThorLabs breadboard. Attached is the V-block holding the proximal end of the specimen, along with the camera to capture high resolution video during testing

A wet-mist suppression system (using an aqueous solution of 9gm/L NaCl and 31mL/L of an anticorrosion organic oil additive) was also integrated into the environmental chamber to: 1) suppress airborne micro-particulates which may develop during testing, 2) appropriately hydrate the bone tissue during testing, and 3) mitigate rust development. Vertical deflection at the load point was recorded automatically as crosshead movement

from the load frame system (830AT, TestResources, Shakopee, Minnesota). Of specific concern to these experiments is the degree of gapping at the replicated fracture location. This was optically measured using a high definition camera (Vixia HF R600, Canon, Tokyo, Japan) positioned in front of the experimental setup and analyzed using image processing software (ImageJ, U.S. National Institutes of Health, Bethesda, Maryland). A high-speed camera system (i-Speed, Olympus Corporation, Tokyo, Japan) was positioned behind the high definition camera so that the same area of interest could be captured for failure analysis [Figure 30].

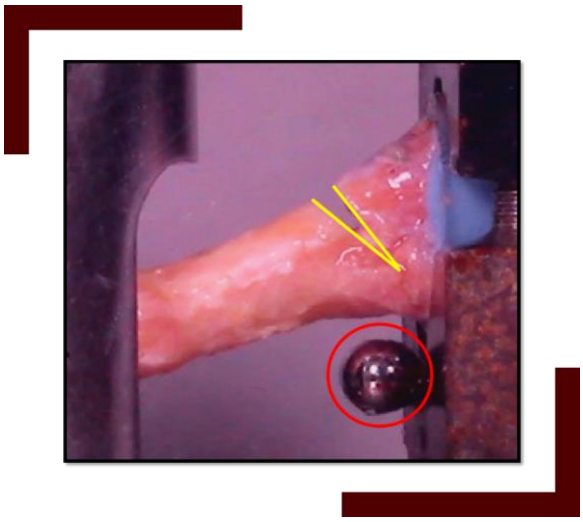

Figure 30: Optical gap measurement - the ball bearing was used as a reference metric

Cyclic cantilever failure tests were performed in a medial-lateral bending application to replicate the number of cycles and increases in loading experienced postoperatively. The load was applied to the distal end in a gradient-cycle method (i.e. incrementally increasing

load amplitude in the medial direction). All cyclical tests were conducted under sinusoidal load control parameters at a constant frequency of 0.25Hz, with load and displacement data collected. Testing was concluded once each specimen had completed the prescribed cycle count or experienced a catastrophic mechanical failure of the plate, screw, or bone. Critical testing events such as one millimeter gap development at the fracture location (clinical failure criteria) were also recorded. Additionally, failure mode, number of cycles to failure (CTF), peak failure load (PFL), and gap width (GW) video were recorded for each specimen. While the clinical failure was defined with respect to the GW, the catastrophic mechanical failure was defined as a fracture of the bone or device. All devices were tested to catastrophic mechanical failure.

A preload of 2.5 lbf [11.1N] was applied to the setup prior to taking deflection measurements. The preload removed compliance from the setup and seated the fixture to the test specimen. Following application of the preload protocol, a graded cyclic fatigue protocol was initiated wherein the load was varied from zero to some target maximum value for 10 cycles at 0.25Hz. The target maximum value was increased by 5.0lbf [22.2N] following each round of 10 cycles. Specifically, for the first round of 10 cycles the load was varied in a sinusoidal manner from zero to a target maximum of 5.0lbf [22.2N]. In the second round the load was varied from zero to a target maximum of 10.0lbf [44.4N]. For each successive round, the target maximum was increased by 5.0lbf [22.2N]. There was no delay between rounds, testing was continuous until failure, i.e. transitions from one

round to the next were seamless [Figure 31]. Testing was concluded once each specimen had experienced catastrophic mechanical failure of the implant or bone.

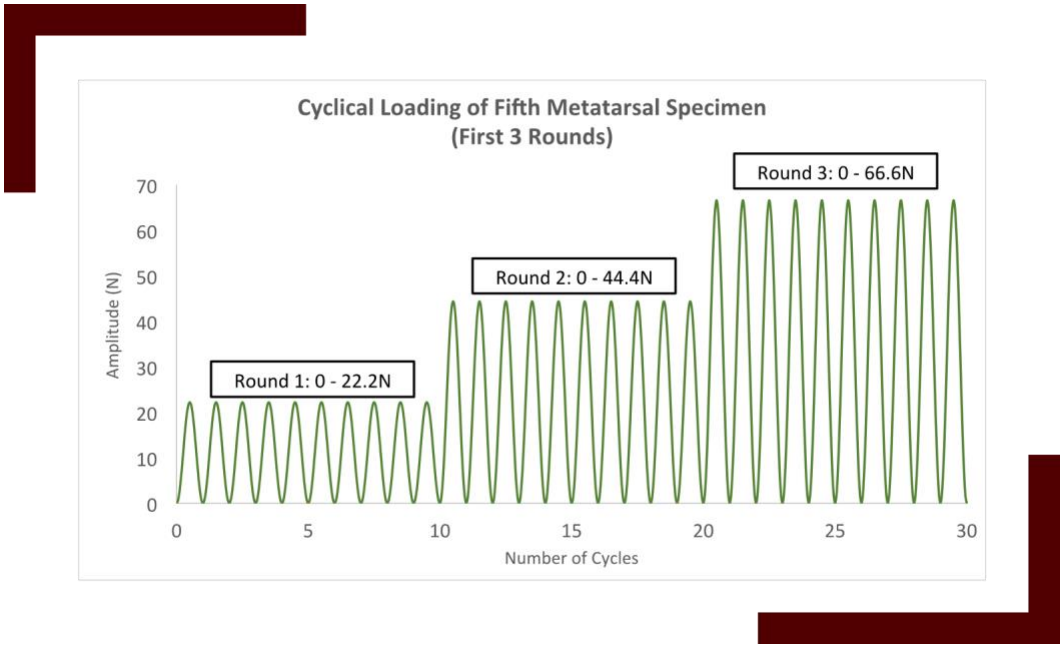

Figure 31: Illustration of the first three rounds of the cyclic loading protocol - the maximum load was increased by 22.2 N in each successive round

3.2.3 Results

All samples were tested to catastrophic failure, which predominantly occurred at the bone implant interface. There was a significant difference found between the plate and screw groups with regard to CTF (63.9 vs 37.3 P=0.01), PFL (35.8 lbf vs 21.7 lbf, P=0.01), and GW (0.0mm vs 3.2mm, P=<0.01) respectively reported as means.

Continuous optical measurement of the fracture GW revealed that 40% of the screw samples had failed according to clinical standards (measured gap increase of one millimeter or more) within the first round (10 cycles) of loading. In contrast, none of the plate samples failed in this round. By the end of the second round of loading (20 cycles), over half of the screws had demonstrated clinical failure while only one of the plate samples had failed. By the end of the third round of loading (30 cycles), all screw samples had failed according to the clinical failure criteria. No additional plate samples failed under the same conditions (Figure 6b).

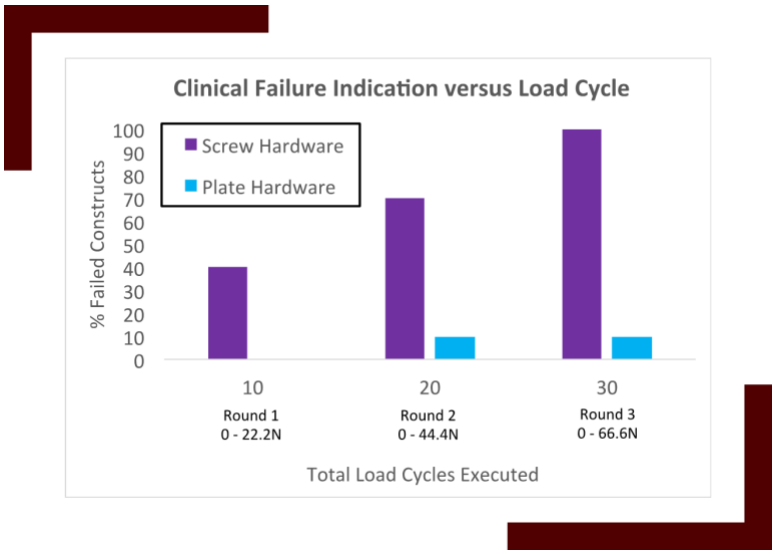

Figure 32: This graft shows the cumulative percent of each group demonstrating clinical failure (as indicated by a fracture gap increase of 1mm), versus loading round as indicated by number of cycles (10 cycles per round); the maximum applied load was increased by 5.0 lbf [22.2 N] in each successive round

Note that all screw samples exhibited clinical failure at bending moments greater than 2.5 Nm. Furthermore, all screw samples exhibited catastrophic failure at bending moments less than 8 Nm [Figure 32]. All but one of the plate samples failed catastrophically prior to reaching the clinical failure criteria. This one plate failure occurred within the second round of loading.

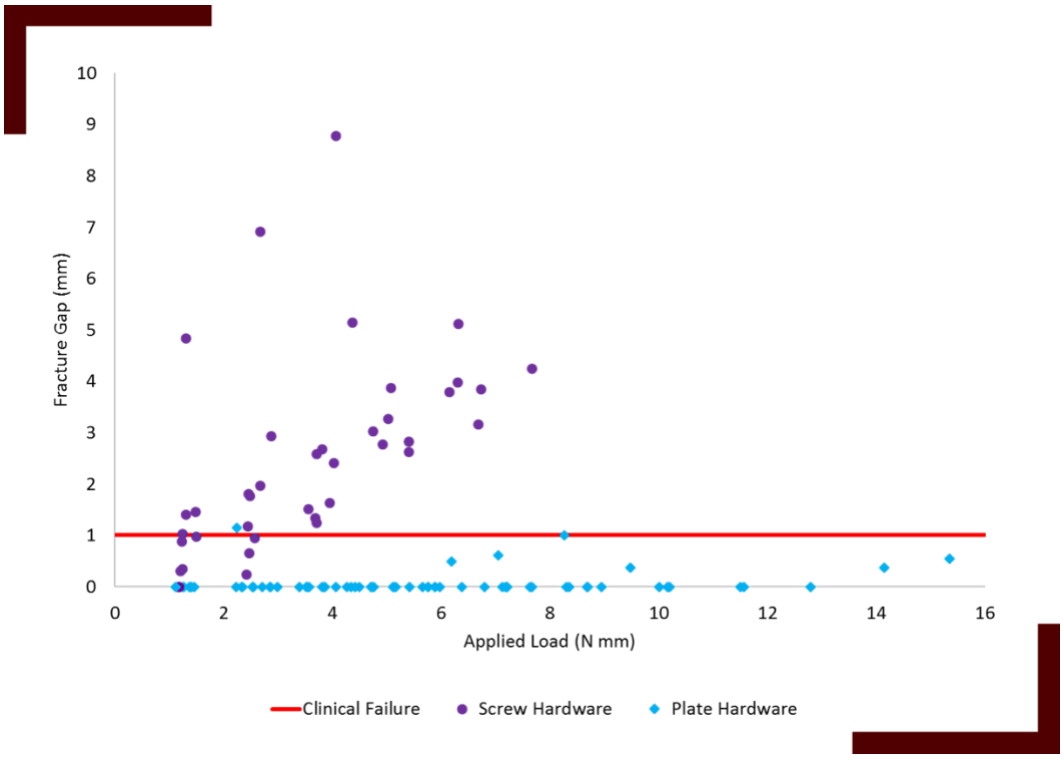

Figure 33: Illustration of the GW measurement during each round of loading versus the applied bending moment where the red line demarcates the clinical failure criteria used for this study

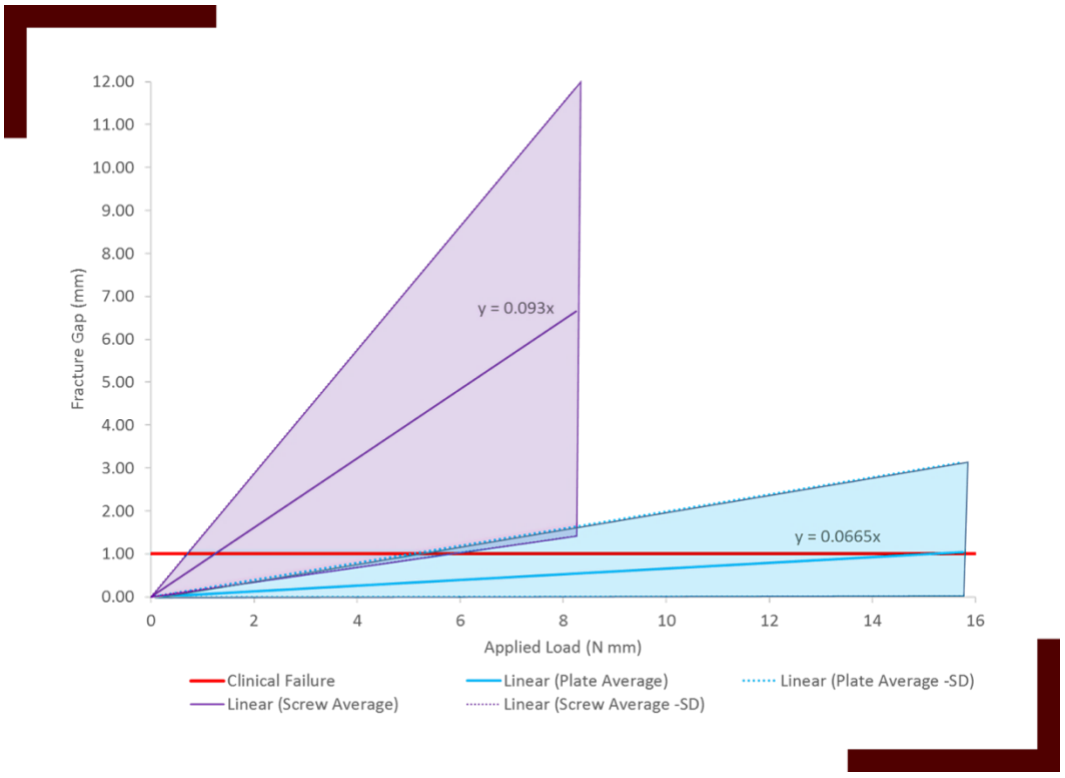

Figure 34: Illustration of a linear curve fit of the data for each sample plotting the average slope of these fits for the respective screw and plate samples; the shaded region indicates one standard deviation

Based on the lower deflection angles observed, the bone-plate constructs exhibited a greater bending stiffness than the bone-screw constructs (Figure 8a). Increasing the load results in an increase in the deflection angle. Thus, at higher loads the angle of deflection observed in the bone-plate constructs may be similar to that observed in the bone-screw constructs at lower loads. At similar angles of deflection, the measured gap is higher in the screw samples than the plate samples (Figure 8b). Thus, fractures repaired with the plate device are both more resistant to bending at a given load and more resistant to

widening of the fracture gap at similar deflection angles, i.e. under similar bending conditions.

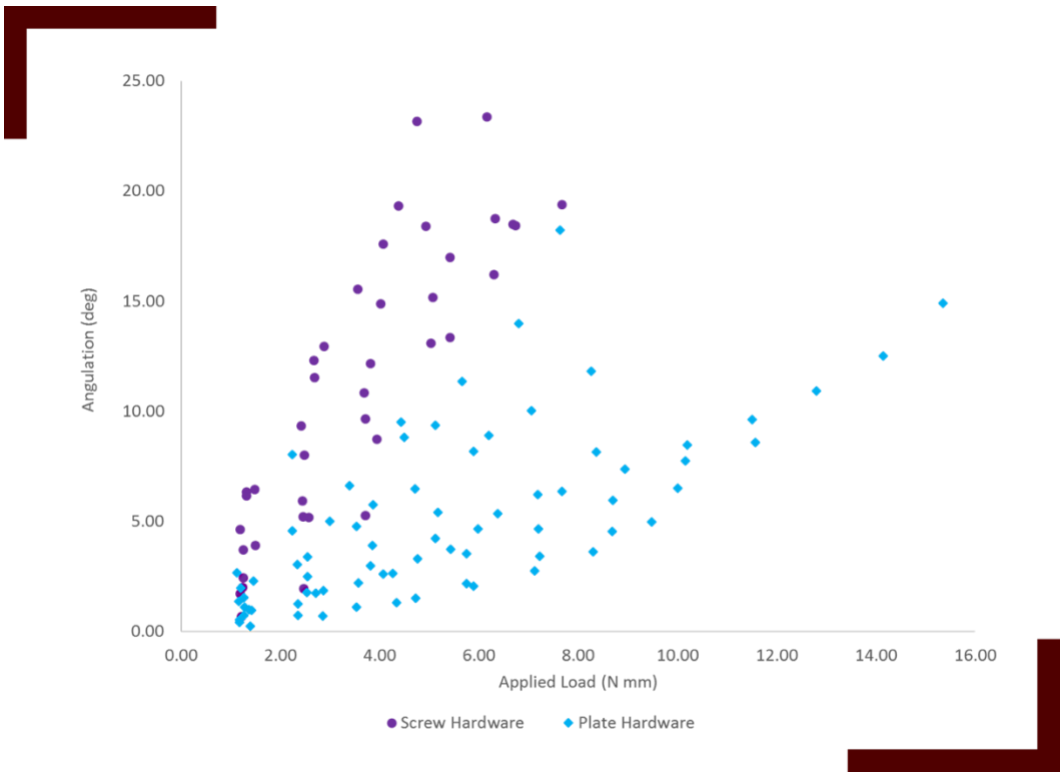

Figure 35: Illustration of the angular deflection of samples in response to the bending moment; the vertical deflection is a measure of the bending in the bone-device construct

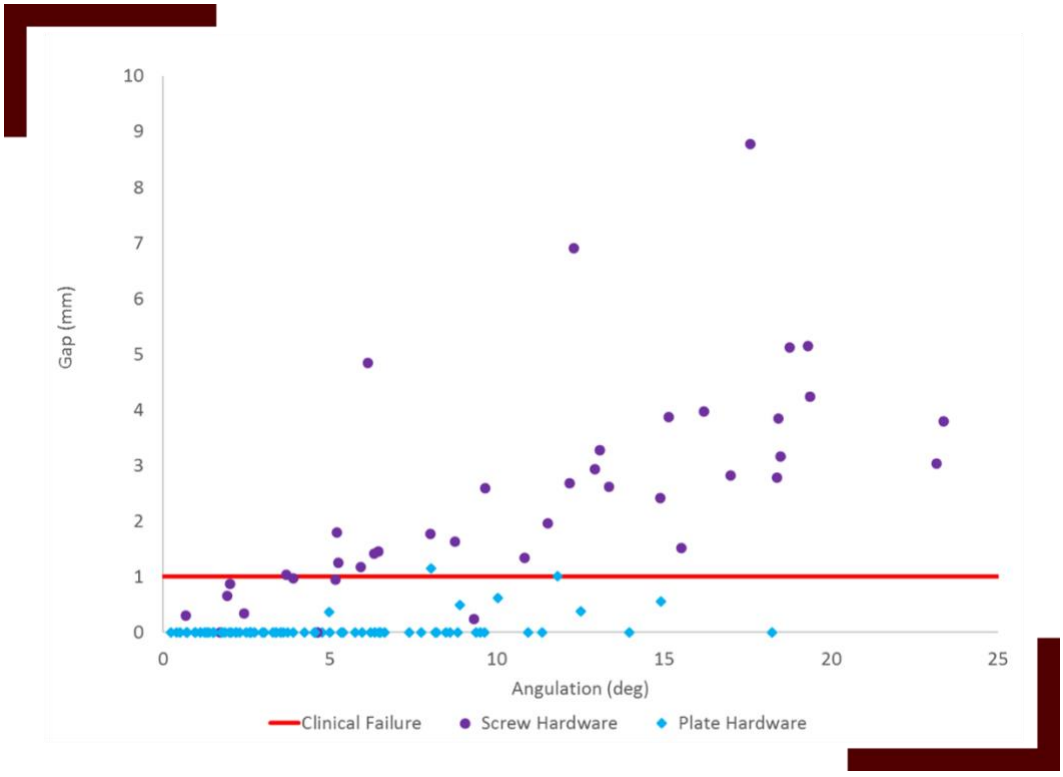

Figure 36: Correlation of fracture gapping to angular deflection

3.1.4 Discussion

This biomechanical investigation demonstrated plantar-lateral plating is significantly stronger than an intramedullary screw for Jones fracture fixation, confirming the hypothesis. Larger CTF and PFL along with smaller GW were recognized in the plate group compared to the screw group, which may hold clinical importance in both primary and revision Jones fracture treatments. Due to the cyclic nature of the loading protocol, reporting PFL alone (clinical or catastrophic) would be misleading as some samples actually crossed the failure threshold at low loads within a given high load cycle. For

example, one sample may fail at 20N within the first cyclic loading round (0-22.2N) while another sample might fail at 5N within the fourth cyclic loading round (0-88.8N), i.e. after being subjected to very high loads relative to the first sample. Thus, we are reporting CTF as well.

Multiple studies, both clinical and biomechanical, have investigated different screw constructs with varying sizes, orientations, and materials [46, 49, 56, 69, 70]. A 5.5 mm diameter screw has been suggested to be an adequate size and has shown to be successful in treating these fractures [49, 68, 71]. Sides et al performed a similar biomechanical study using paired cadaver feet to compare cantilever bending strength and pullout strength of a partially threaded solid screw to a cannulated tapered variable pitch screw, finding no significant ($P>0.05$) difference in bending strength but significantly ($P=0.001$) higher pullout strength in the solid partially threaded screw [46]. The authors chose to separate the paired feet by placing the solid partially threaded screw in all right foot specimens, and the cannulated tapered variable pitch screw in all the left foot specimens [46]. The current study compared a similar partially threaded solid screw to a low-profile locking plate. However, this study assigned separation of the paired feet randomly by placing the partially threaded screw as well as the plate in an equal amount of left and right feet while keeping them paired. The current mechanical testing in this study was similar to Sides et al investigation since it also cleared the bone of all soft tissue then used an epoxy to hold the bone specimens in place for testing in the machine.

Shah et al performed a biomechanical study comparing 4.5 mm and 5.5 mm diameter cannulated screws for fixation of a replicated Jones fracture in cadaver fifth metatarsal specimens showing no statistical difference ($P>0.05$) in strength when subjected to a three-point bending load [68]. The failure in all the specimens was ultimately by penetration of the distal screw threads through the superior cortex of the fifth metatarsal distal to the replicated fracture [68]. One inherent weakness of the study pointed out by Shah et al was related to the three-point bending load model's inability to mimic physiologic loading on the fifth metatarsal specimens [68]. Therefore, this study used a cantilever loading protocol thought to be more capable of reproducing the natural physiologic stresses that create the fracture gap during activity.

This loading scenario was determined to be more physiologically relevant, as opposed to a linear failure test due to the type of loading the foot incurs during normal human ambulation. By increasing the amplitude, maximum loads can be reached to better replicate the physiologic forces that occur in the foot during high demand athletic activities. The medial-lateral loading direction was chosen because the mechanism of Jones fracture injury has long been understood to involve forces acting on the lateral border of the forefoot [47, 55]. Donahue and Sharkey found both average and peak strains on the lateral cortex of the fifth metatarsal to exceed those measured on the dorsum of the metatarsal [50, 57]. In addition, Jones fracture non-unions and fixation failures are manifested by prominent lateral gapping, clearly indicating medial angulation of the distal fragment.

Force-plate analysis has shown that a vertical or a medial lateral force typically occurs at the time of fracture [55]. Whereas an inversion injury typically occurs during tuberosity avulsion fractures but does not appear to be a main component of the injury distal to the tuberosity. Therefore, the authors did not feel that reproduction of the inversion force was necessary.

Choi et al. described good results using hook plate fixation for fifth metatarsal base fractures with only one patient requiring hardware removal due to irritation, and all fractures reaching bony union [61]. The authors feel that the straight locking plate used in the current study is even less prominent than a hook plate, and since the plate is placed in a more plantar location, it may cause less irritation.

Early return to play in athletes prior to full radiographic union has been associated with an increased risk of failure after intramedullary screw fixation [45, 57]. To the author's knowledge, no studies have been performed specifically investigating if this holds true for open reduction internal fixation with a locking plate construct. Further clinical outcome studies are warranted with regard to Jones fracture management using plantar-lateral plating. However, the authors feel the results of this study do show that this procedure is a superior fixation technique for both revision and primary procedures involving fractures of the proximal fifth metatarsal.

An inherent weakness associated with biomechanical testing is that the specimen is often devoid of all ligamentous, tendinous, and soft tissue attachments which would add natural

stability to the bone as stresses were applied. Again the authors felt that leaving any ligamentous, tendinous, or soft tissue attachments may create an unacceptable difference between the matched pairs of specimens. For this comparative study, it is not likely that including such factors would alter the results in any significant manner.

The method this investigation used in creating an osteotomy with a microsagittal saw was similar to the previously mentioned studies [46, 68]. Unfortunately, a saw osteotomy is not the same as an actual fracture therefore this can be noted as a weakness as well. However, this method was chosen in order to reproduce the same defect location and angulations on all specimens. The authors felt that if an actual fracture was created instead of an osteotomy this would lead to unacceptable differences between matched pairs of specimens.

3.2.5 Conclusion

This biomechanical investigation demonstrated plantar-lateral plating is significantly stronger than intramedullary screw Jones fracture fixation. Larger CTF and PFL along with smaller GW were recognized in the plate group compared to the screw group.

4. CONCLUSION

This research, which would not have been possible without multidisciplinary assistance and collaboration from the medical, veterinary, and engineering fields, demonstrates the effectiveness of the One Health initiative. By working closely with veterinary professionals, a novel cost effective Joint Motion Replicator was designed and built which closely mimics dynamic loading conditions. The JMR was then utilized for a comparative study of implantable devices designed to treat hip luxation in canines. Similarly, collaboration with medical professionals led to the creation of a mechanical test system and environmental chamber that was used to analyze the effectiveness of an intramedullary screw and plantar-lateral plating construct to treat Jones Fractures in paired cadaver foot specimens.

Test results revealed that the JMR is effective in modeling a variety of physiologic systems and is a valid alternative to more expensive specialized replicators currently available, as well as providing the ability to be easily modified for use in diverse applications. Toggle suture constructs that were then studied using the JMR revealed that the Tightrope suture construct performed better than both the Ethibond and Monofilament Nylon suture constructs. Tightrope constructs experienced the least amount of failures and were able to consistently resist the greatest number of both F/E and A/A cycles.

The biomechanical investigation comparing the intramedullary screw with the plantar-lateral plating construct showed that the plantar-lateral plate was significantly superior for

treating Jones Fractures, requiring larger loads to reach catastrophic failure and also larger peak failure loads. In addition, smaller gap widths appeared in the samples utilizing the plantar-lateral plate, which is also of clinical importance. Based on these results, it is likely that replacing the intramedullary screw fracture fixation technique with the plantar-lateral plate will result in decreased risk of delayed unions, nonunions, and refractures. Further research would be required to explore the extent of benefit to athletes and other active individuals that experience these particular fractures.

REFERENCES

[1] O. Health. (2017). *One Health Initiative*. Available: http://www.onehealthinitiative.com/index.php

[2] C. Liu, S. M. Green, N. D. Watkins, P. J. Gregg, and A. W. McCaskie, "A preliminary hip joint replicator study of the migration of a cemented femoral stem," *Proc Inst Mech Eng H,* vol. 217, pp. 127-35, 2003.

[3] L. D. Noble, Jr., R. W. Colbrunn, D. G. Lee, A. J. van den Bogert, and B. L. Davis, "Design and validation of a general purpose robotic testing system for musculoskeletal applications," *J Biomech Eng,* vol. 132, p. 025001, Feb 2010.

[4] A. Ni Annaidh, M. Destrade, M. D. Gilchrist, and J. G. Murphy, "Deficiencies in numerical models of anisotropic nonlinearly elastic materials," *Biomech Model Mechanobiol,* vol. 12, pp. 781-91, Aug 2013.

[5] Y. Chen, M. Pani, F. Taddei, C. Mazza, X. Li, and M. Viceconti, "Large-scale finite element analysis of human cancellous bone tissue micro computer tomography data: a convergence study," *J Biomech Eng,* vol. 136, p. 101013, Oct 2014.

[6] K. Lekadir, C. Noble, J. Hazrati-Marangalou, C. Hoogendoorn, B. van Rietbergen, Z. A. Taylor, *et al.*, "Patient-Specific Biomechanical Modeling of Bone Strength Using Statistically-Derived Fabric Tensors," *Ann Biomed Eng,* vol. 44, pp. 234-46, Jan 2016.

[7] M. Ali, M. Al-Hajjar, S. Partridge, S. Williams, J. Fisher, and L. M. Jennings, "Influence of hip joint replicator design and mechanics on the wear and creep of metal-on-polyethylene bearings," *Proc Inst Mech Eng H,* vol. 230, pp. 389-97, May 2016.

[8] G. D. Langohr, G. S. Athwal, J. A. Johnson, and J. B. Medley, "Wear simulation strategies for reverse shoulder arthroplasty implants," *Proc Inst Mech Eng H,* vol. 230, pp. 458-69, May 2016.

[9] M. Lowry, H. Rosenbaum, and P. S. Walker, "Evaluation of total knee mechanics using a crouching replicator with a synthetic knee substitute," *Proc Inst Mech Eng H,* vol. 230, pp. 421-8, May 2016.

[10] X. Roussignol, C. Siedlecki, F. Duparc, F. Dujardin, and M. Ould-Slimane, "Do temperature variations at the bearing surface during gait affect polyethylene wear

in Charnley low-friction arthroplasty of the hip? Replicator study comparing UHMWPE and highly cross-linked polyethylene," *Orthop Traumatol Surg Res,* Jun 15 2016.

[11] S. L. Affatato, W.; Zavalloni M., "Hip Joint Replicators: State of the Art," in *Tribology,* ed, 2008, pp. 171-179.

[12] P. S. M. Barbour, M. H. Stone, and J. Fisher, "A hip joint replicator study using simplified loading and motion cycles generating physiologic wear paths and rates," *Proceedings of the Institution of Mechanical Engineers, Part H: Journal of Engineering in Medicine,* vol. 213, pp. 455-467, 1999.

[13] A. A. Goldsmith and D. Dowson, "Development of a ten-station, multi-axis hip joint replicator," *Proc Inst Mech Eng H,* vol. 213, pp. 311-6, 1999.

[14] J. B. Medley, J. J. Krygier, J. D. Bobyn, F. W. Chan, A. Lippincott, and M. Tanzer, "Kinematics of the MATCO hip replicator and issues related to wear testing of metal-metal implants," *Proc Inst Mech Eng H,* vol. 211, pp. 89-99, 1997.

[15] L. P. Maletsky and B. M. Hillberry, "Simulating dynamic activities using a five-axis knee replicator," *J Biomech Eng,* vol. 127, pp. 123-33, Feb 2005.

[16] Y. C. Fu, B. T. Torres, and S. C. Budsberg, "Evaluation of a three-dimensional kinematic model for canine gait analysis," *Am J Vet Res,* vol. 71, pp. 1118-22, Oct 2010.

[17] P. D. Fry, "Observations on the surgical treatment of hip dislocation in the dog and cat," *J Small Anim Pract,* vol. 15, pp. 661-70, Nov 1974.

[18] J. A. Johnston, C. Austin, and G. J. Breur, "Incidence of canine appendicular musculoskeletal disorders in 16 veterinary teaching hospitals from 1980 through 1989," vol. v. 7, 1994.

[19] B. S. Beale, D. D. Lewis, R. B. Parker, G. C. Mac-pherson, and C. A. Kuntz, "Ischioilial pinning for stabilization of hip luxations in twenty-one dogs: a retrospective evaluation," *Vet Comp Orthop Traumatol,* vol. 4, pp. 34-40, 1991.

[20] J. L. Demko, B. K. Sidaway, K. M. Thieman, D. B. Fox, C. R. Boyle, and R. M. McLaughlin, "Toggle rod stabilization for treatment of hip joint luxation in dogs: 62 cases (2000-2005)," *J Am Vet Med Assoc,* vol. 229, pp. 984-9, Sep 15 2006.

[21] A. T. Knowles, J. O. Knowles, and R. P. Knowles, "An operation to preserve the continuity of the hip joint," *J Am Vet Med Assoc,* pp. 508-515, 1953.

[22] D. D. Lawson, "Toggle fixation for recurrent dislocation of the hip in the dog," *J Sm Anim Prac,* pp. 57-59, 1964.

[23] S. R. Duff and D. Bennett, "Hip luxation in small animals: an evaluation of some methods of treatment," *Vet Rec,* vol. 111, pp. 140-3, Aug 14 1982.

[24] D. Bennett and S. R. Duff, "Transarticular pinning as a treatment for hip luxation in the dog and cat," *J Small Anim Pract,* vol. 21, pp. 373-9, Jul 1980.

[25] B. P. Meij, H. A. W. Hazewinkel, and R. C. Nap, "Results of extra-articular stabilisation following open reduction of coxofemoral luxation in dogs and cats," *Journal of Small Animal Practice,* vol. 33, pp. 320-326, 1992.

[26] J. J. Haburjak, T. M. Lenehan, J. Harari, R. Gurevitch, B. Rivers, G. B. Tarvin, *et al.*, "Treatment of traumatic hip luxation with triple pelvic osteotomy in 19 dogs (1987-1999)," *Vet Comp Orthop Traumatol,* pp. 69-77, 2001.

[27] E. Kilic, I. Ozaydin, G. Atalan, and V. Baran, "Transposition of the sacrotuberous ligament for the treatment of coxofemoral luxation in dogs," *J Small Anim Pract,* vol. 43, pp. 341-4, Aug 2002.

[28] M. Zakiewicz, "Recurrent hip luxation in the dog: skin as substitute ligament," *Vet Rec,* vol. 81, pp. 538-9, Nov 18 1967.

[29] H. P. Beckham, M. M. Smith, and D. A. Kern, "Use of a modified toggle pin for repair of coxofemoral luxation in dogs with multiple orthopedic injuries: 14 cases (1986-1994)," *J Am Vet Med Assoc* pp. 81-84, 1996.

[30] H. R. Denny and H. M. Minter, "Recurrent coxofemoral luxation in the dog," *Vet Annual,* pp. 220-225, 1973.

[31] M. F. Flynn, D. N. Edmiston, S. C. Roe, D. C. Richardson, D. J. DeYoung, and C. F. Abrams, Jr., "Biomechanical evaluation of a toggle pin technique for management of coxofemoral luxation," *Vet Surg,* vol. 23, pp. 311-21, Sep-Oct 1994.

[32] D. L. Piermattei, "A technique for surgical management of coxofemoral luxations," *Sm Anim Clin,* pp. 373-386, 1963.

[33] M. G. Serdy, K. S. Schulz, W. Hornof, C. Koehler, D. Chiu, and P. B. Vasseur, "Closed toggle pinning for canine traumatic coxofemoral luxation," vol. v. 12, 1999.

[34] D. Spranklin, S. Elder, C. Boyle, and R. McLaughlin, "Comparison of a suture anchor and a toggle rod for use in toggle pin fixation of coxofemoral luxations," *J Am Anim Hosp Assoc*, vol. 42, pp. 121-6, Mar-Apr 2006.

[35] W. I. Baltzer, K. S. Schulz, S. M. Stover, K. T. Taylor, and P. H. Kass, "Biomechanical analysis of suture anchors and suture materials used for toggle pin stabilization of hip joint luxation in dogs," *Am J Vet Res*, vol. 62, pp. 721-8, May 2001.

[36] S. Jha and M. P. Kowaleski, "Mechanical analysis of twelve toggle suture constructs for stabilization of coxofemoral luxations," *Vet Surg*, vol. 41, pp. 948-53, Nov 2012.

[37] I. IMEX Veterinary. (2016). *Stabilization of coxofemoral luxation using the toggle pin method*. Available: http://www.imexvet.com/learn/technical-articles/stabilization-coxofemoral-luxation-using-toggle-pin-method

[38] M. F. Flynn. *Toggle-rod fixation for management of coxofemoral luxation-technique and tips*. Available: http://www.securos.com/ProductInstructions/CoxofemoralLuxationManagementInstructions2.aspx

[39] C. B. Chan, M. Spierenburg, S. L. Ihle, and C. Tudor-Locke, "Use of pedometers to measure physical activity in dogs," *J Am Vet Med Assoc*, vol. 226, pp. 2010-5, Jun 15 2005.

[40] S. C. Budsberg, M. C. Verstraete, and R. W. Soutas-Little, "Force plate analysis of the walking gait in healthy dogs," *Am J Vet Res*, vol. 48, pp. 915-8, Jun 1987.

[41] P. F. Rumph, J. E. Lander, S. A. Kincaid, D. K. Baird, J. R. Kammermann, and D. M. Visco, "Ground reaction force profiles from force platform gait analyses of clinically normal mesomorphic dogs at the trot," *Am J Vet Res*, vol. 55, pp. 756-61, Jun 1994.

[42] M. Silva, "Bone Mechanical Testing by Three-Point Bending," *Musculoskeletal Structure and Strength Core*, 2016.

[43] PolyScience. (2015). *Model 210 Heated Recirculator*. Available: https://www.polyscience.com/circulating-baths/model-210-heated-recirculator-0

[44] T. B. Dameron, Jr., "Fractures of the Proximal Fifth Metatarsal: Selecting the Best Treatment Option," *J Am Acad Orthop Surg*, vol. 3, pp. 110-114, Mar 1995.

[45] M. P. Pietropaoli, D. C. Wnorowski, F. W. Werner, and M. D. Fortino, "Intramedullary screw fixation of Jones fractures: a biomechanical study," *Foot Ankle Int,* vol. 20, pp. 560-3, Sep 1999.

[46] M. T. Glasgow, R. J. Naranja, Jr., S. G. Glasgow, and J. S. Torg, "Analysis of failed surgical management of fractures of the base of the fifth metatarsal distal to the tuberosity: the Jones fracture," *Foot Ankle Int,* vol. 17, pp. 449-57, Aug 1996.

[47] G. A. Rosenberg and J. J. Sferra, "Treatment strategies for acute fractures and nonunions of the proximal fifth metatarsal," *J Am Acad Orthop Surg,* vol. 8, pp. 332-8, Sep-Oct 2000.

[48] T. S. Mologne, J. M. Lundeen, M. F. Clapper, and T. J. O'Brien, "Early screw fixation versus casting in the treatment of acute Jones fractures," *Am J Sports Med,* vol. 33, pp. 970-5, Jul 2005.

[49] D. A. Porter, A. M. Rund, R. Dobslaw, and M. Duncan, "Comparison of 4.5- and 5.5-mm cannulated stainless steel screws for fifth metatarsal Jones fracture fixation," *Foot Ankle Int,* vol. 30, pp. 27-33, Jan 2009.

[50] J. D. Granata, G. C. Berlet, T. M. Philbin, G. Jones, C. C. Kaeding, and K. S. Peterson, "Failed Surgical Management of Acute Proximal Fifth Metatarsal (Jones) Fractures: A Retrospective Case Series and Literature Review," *Foot Ankle Spec,* vol. 8, pp. 454-9, Dec 2015.

[51] J. H. Kavanaugh, T. D. Brower, and R. V. Mann, "The Jones fracture revisited," *J Bone Joint Surg Am,* vol. 60, pp. 776-82, Sep 1978.

[52] K. J. Hunt and R. B. Anderson, "Treatment of Jones fracture nonunions and refractures in the elite athlete: outcomes of intramedullary screw fixation with bone grafting," *Am J Sports Med,* vol. 39, pp. 1948-54, Sep 2011.

[53] A. J. Roche and J. D. Calder, "Treatment and return to sport following a Jones fracture of the fifth metatarsal: a systematic review," *Knee Surg Sports Traumatol Arthrosc,* vol. 21, pp. 1307-15, Jun 2013.

[54] M. Fernandez Fairen, J. Guillen, J. M. Busto, and J. Roura, "Fractures of the fifth metatarsal in basketball players," *Knee Surg Sports Traumatol Arthrosc,* vol. 7, pp. 373-7, 1999.

[55] C. D. Murawski and J. G. Kennedy, "Percutaneous internal fixation of proximal fifth metatarsal jones fractures (Zones II and III) with Charlotte Carolina screw

and bone marrow aspirate concentrate: an outcome study in athletes," *Am J Sports Med,* vol. 39, pp. 1295-301, Jun 2011.

[56] R. W. Wright, D. A. Fischer, R. A. Shively, R. S. Heidt, Jr., and G. W. Nuber, "Refracture of proximal fifth metatarsal (Jones) fracture after intramedullary screw fixation in athletes," *Am J Sports Med,* vol. 28, pp. 732-6, Sep-Oct 2000.

[57] C. M. Larson, L. C. Almekinders, T. N. Taft, and W. E. Garrett, "Intramedullary screw fixation of Jones fractures. Analysis of failure," *Am J Sports Med,* vol. 30, pp. 55-60, Jan-Feb 2002.

[58] G. Ochenjele, B. Ho, P. J. Switaj, D. Fuchs, N. Goyal, and A. R. Kadakia, "Radiographic study of the fifth metatarsal for optimal intramedullary screw fixation of Jones fracture," *Foot Ankle Int,* vol. 36, pp. 293-301, Mar 2015.

[59] J. H. Choi, K. T. Lee, Y. K. Lee, J. Y. Lee, and H. R. Kim, "Surgical results of zones I and II fifth metatarsal base fractures using hook plates," *Orthopedics,* vol. 36, pp. e71-4, Jan 2013.

[60] J. T. Johnson, S. A. Labib, and R. Fowler, "Intramedullary screw fixation of the fifth metatarsal: an anatomic study and improved technique," *Foot Ankle Int,* vol. 25, pp. 274-7, Apr 2004.

[61] F. Horst, B. J. Gilbert, R. R. Glisson, and J. A. Nunley, "Torque resistance after fixation of Jones fractures with intramedullary screws," *Foot Ankle Int,* vol. 25, pp. 914-9, Dec 2004.

[62] J. Huh, R. R. Glisson, T. Matsumoto, and M. E. Easley, "Biomechanical Comparison of Intramedullary Screw Versus Low-Profile Plate Fixation of a Jones Fracture," *Foot Ankle Int,* vol. 37, pp. 411-8, Apr 2016.

[63] I. P. Kelly, R. R. Glisson, C. Fink, M. E. Easley, and J. A. Nunley, "Intramedullary screw fixation of Jones fractures," *Foot Ankle Int,* vol. 22, pp. 585-9, Jul 2001.

[64] S. N. Shah, G. O. Knoblich, D. P. Lindsey, J. Kreshak, S. A. Yerby, and L. B. Chou, "Intramedullary screw fixation of proximal fifth metatarsal fractures: a biomechanical study," *Foot Ankle Int,* vol. 22, pp. 581-4, Jul 2001.

[65] V. Mahajan, H. W. Chung, and J. S. Suh, "Fractures of the proximal fifth metatarsal: percutaneous bicortical fixation," *Clin Orthop Surg,* vol. 3, pp. 140-6, Jun 2011.

[66] J. D. Orr, R. R. Glisson, and J. A. Nunley, "Jones fracture fixation: a biomechanical comparison of partially threaded screws versus tapered variable pitch screws," *Am J Sports Med,* vol. 40, pp. 691-8, Mar 2012.

[67] J. Metzl, K. Olson, W. H. Davis, C. Jones, B. Cohen, and R. Anderson, "A clinical and radiographic comparison of two hardware systems used to treat jones fracture of the fifth metatarsal," *Foot Ankle Int,* vol. 34, pp. 956-61, Jul 2013.

[68] S. D. Sides, N. L. Fetter, R. Glisson, and J. A. Nunley, "Bending stiffness and pull-out strength of tapered, variable pitch screws, and 6.5-mm cancellous screws in acute Jones fractures," *Foot Ankle Int,* vol. 27, pp. 821-5, Oct 2006.

[69] S. W. Donahue, N. A. Sharkey, K. A. Modanlou, L. N. Sequeira, and R. B. Martin, "Bone strain and microcracks at stress fracture sites in human metatarsals," *Bone,* vol. 27, pp. 827-33, Dec 2000.

[70] S. Rammelt, J. Heineck, and H. Zwipp, "Metatarsal fractures," *Injury,* vol. 35 Suppl 2, pp. SB77-86, Sep 2004.

[71] A. M. Fansa, N. A. Smyth, C. D. Murawski, and J. G. Kennedy, "The lateral dorsal cutaneous branch of the sural nerve: clinical importance of the surgical approach to proximal fifth metatarsal fracture fixation," *Am J Sports Med,* vol. 40, pp. 1895-8, Aug 2012.